Runx2 and Vascular Calcification

Theodore Chen

A dissertation
submitted in partial fulfillment of the
requirements for the degree of

Doctor of Philosophy

University of Washington

2016

Reading Committee:
Yanfeng (Mei) Speer, Co-chair
Cecilia M. Giachelli, Co-chair
Marta Scatena

Program Authorized to Offer Degree:
Department of Bioengineering

University of Washington

Abstract

Runx2 and Vascular Calcification

Theodore Ming-Chien Chen

Co-chairs of the Supervisory Committee:
Research Associate Professor Yanfeng (Mei) Speer
Professor Cecilia M. Giachelli
Department of Bioengineering

Complications arising from vascular calcification, the inappropriate deposition of calcium phosphate crystals in the vasculature, have become more evident in recent years as human longevity has increased. Arterial calcification is frequently categorized as two types, depending on where it occurs: arterial medial calcification (AMC), commonly associated with aging, type 2 diabetes mellitus, and CKD, and arterial intimal calcification (AIC), characterized by plaque accumulation and occlusive lesions in the vasculature. Runx2 (runt-related transcription factor 2) is a critical regulator of bone development, early chondrocyte proliferation, and hypertrophic chondrocyte formation. Surprisingly, Runx2 has been found to be upregulated in arteries of patients with atherosclerosis (intimal calcification) and CKD (medial calcification). Because SMCs can undergo lineage reprogramming toward osteoblastic and chondrocytic fates during

vascular calcification, we propose to determine whether SMC-specific Runx2 expression is required for development of AMC and AIC.

We developed a mouse with smooth muscle-specific removal of Runx2 (Runx2$^{\Delta SM}$). We observed that in AMC, Runx2 was required for pathological AMC development and prevented osteogenic phenotype change. Similar to our *in vivo* experiments, SMCs isolated from Runx2$^{\Delta SM}$ mice were much less susceptible to elevated phosphate-induced calcification. In AIC, on the other hand, Runx2 inhibited not only osteoblastic differentiation of vascular SMCs but also SMC-derived chondrocyte maturation, leading to a 50% reduction in calcification. Our studies showed that while SMC expression of Runx2 was not required for initial chondrogenesis, it was necessary for maturation of chondrocytes to a pro-mineralizing, hypertrophic state.

Lastly, we proposed to investigate the effect of Runx2 on development of atherosclerosis and polarization of lesional macrophages. Removal of Runx2 did not affect monocyte/macrophage recruitment and atherosclerotic lesion size. Within lesions, we observed a strong shift in macrophage polarization toward an M2 polarization in atherosclerotic aortas. Using a co-culture model of vascular SMCs and RAW264.7 cells to study the effect of Runx2-mediated smooth muscle signaling of macrophages, we found significant increases in expression of two M2 markers: MRC1 and IR-1R2. To our knowledge, these results are the first to show that SMCs can directly alter macrophage polarization, and have promising implications for treatments looking to regulate macrophages in atherosclerotic lesions.

Table of Contents

List of Figures

List of Tables

List of Abbreviations

ABC	avidin-biotin complex
ACTA2	smooth muscle alpha (α)-2 actin
AIC	arterial intimal calcification
ALP	alkaline phosphatase
AMC	arterial medial calcification
ANOVA	analysis of variance
ApoE	apolipoprotein E
Arg1	arginase 1
BCA	bicinchoninic acid *or* brachiocephalic artery
BUN	blood urea nitrogen
CAVD	calcific aortic valve disease
CCD	cleidocranial dysplasia
CKD	chronic kidney disease
Col II	type II collagen
Col X	type X collagen
DMEM	Dulbecco's Modified Eagle Medium
DNA	deoxyribonucleic acid
dpc	days post coitum
EMSA	electrophoretic mobility shift assay
ESRD	end-stage renal disease
FBS	fetal bovine serum
FGF23	fibroblast growth factor 23
GAPDH	glyceraldehyde 3-phosphate dehydrogenase
H&E	hematoxylin & eosin
HCl	hydrochloric acid
HFD	high fat diet
IFN-γ	interferon-γ
IgG	immunoglobulin G
IHC	immunohistochemistry
IL-1	interleukin 1
IL-1β	interleukin 1beta
IL-1R1	interleukin 1 receptor type 1
IL-1R2	interleukin 1 receptor type 2
IL-1RA	interleukin 1 receptor antagonist
IL-4	interleukin 4
IL-6	interleukin 6
IL-10	interleukin 10
IL-12B	interleukin 12B
IU	international unit
LDL	low density lipoprotein
LDLr	low density lipoprotein receptor
MMP13	matrix metallopeptidase 13
MRC1	mannose receptor, C type 1
mRNA	messenger ribonucleic acid

NaOH	sodium hydroxide
NC	normal chow
NEAA	non-essential amino acids
NIH	National Institutes of Health
OCN	osteocalcin
OPN	osteopontin
OSE2	osteoblast specific element 2
OSX	osterix
oxLDL	oxidized low-density lipoproteins
PCR	polymerase chain reaction
Pi	inorganic phosphate
PVDF	polyvinylidene fluoride
RANKL	receptor activator of nuclear factor kappa-B ligand
RNA	ribonucleic acid
RNase	ribonuclease
RT-PCR	reverse transcription polymerase chain reaction
Runx1	Runt-related transcription factor 1
Runx2	Runt-related transcription factor 2
$Runx2^{\Delta SM}$	Runt-related transcription factor 2, SM-specific knockout
$Runx2^{f/f}$	Runt-related transcription factor 2, floxed allele
Runx3	Runt-related transcription factor 3
SDS-PAGE	sodium dodecyl sulfate polyacrylamide gel electrophoresis
SMC	smooth muscle cell
SMMHC	smooth muscle myosin heavy chain
Sox2	SRY (sex determining region Y)-box 2
Th1	Type 1 T helper
Th2	Type 2 T helper
TNF	tumor necrosis factor
VC	vascular calcification
VitD	Vitamin D
VSMC	vascular smooth muscle cell
Ym1	chitinase-like 3

1 Chapter 1: Introduction

1.1 Significance

Vascular calcification (VC) has afflicted humans for millennia; instances of VC have even been observed in mummified remains.[1–3] As human longevity has increased due to better quality of life and care, physiological consequences of VC have become more evident. For instance, the presence and extent of calcific aortic valve disease (CAVD) was the single best predictor of disease progression in patients with calcific aortic stenosis.[4,5] Likewise, in patients with end-stage renal disease (ESRD), arterial calcification was a clear predictor of mortality; patients lacking clinically significant calcification had a much higher five-year survival rate (~90%) compared to patients with significant arterial calcification (<50%).[6] Even after adjusting for common confounders (including diabetic status, chronic kidney disease (CKD), hypertension, sex, and age), patients with intimal and medial calcification exhibited a 5-fold and 16-fold increase, respectively, in relative risk of mortality compared to those without vascular calcification.[1,7] Clearly, arterial calcification is profoundly linked with cardiovascular disease and outcome. Although initially considered as a passive degeneration of dead and dying cells, recent evidence supports an active and highly regulated mechanism of VC involving transdifferentiation of cells into osteochondrogenic lineages resembling the bone development process.[1,8,9] Indeed, the presence of true bone with marrow elements has been observed in up to 15% of human calcified arterial lesions, and osteogenic processes have been detected in nearly all calcified arterial segments.[10,11] Both bone- and cartilage-like tissues have been detected in ~60% of stenotic aortic valves.[12–16]

Arterial calcification is frequently categorized into two distinct types: arterial medial calcification (AMC), typical of patients with type 2 diabetes mellitus and CKD, and arterial intimal calcification (AIC), characterized by inflammation and plaque accumulation in the vasculature. AMC is a hallmark of aging, diabetes, and CKD. It is strongly correlated with coronary artery disease and future cardiovascular events.[6,7,17,18] In patients with CKD, increased stiffness of capacitive arteries (including the aorta) as a result of medial calcification was an independent predictor of cardiovascular mortality.[19] In patients with type 2 diabetes mellitus, the presence of medial calcification was associated with a four-fold increase in risk for lower extremity amputation.[7] AIC, on the other hand, is strongly associated with atherosclerosis and positively correlated with increased plaque burden, plaque instability, and risk of myocardial infarction and stroke.[20–24] Most notably, AIC is characterized by occlusion of the lumen due to an outward remodeling lesion, directly affecting hemodynamics and vessel elastance.[1] A chronic inflammatory disease, atherosclerosis is the most common cause of heart attack and stroke and is the leading cause of death worldwide, accounting for one in three deaths in the US alone.[25,26] Mortality from atherosclerosis can stem from the rupture of unstable plaques, leading to thrombosis and subsequent myocardial infarction and stroke. Since there are no medications targeting lesion regression, it is of particular interest to explicate mechanisms governing plaque stability for development of potential therapeutics for AIC.

1.2 **Runx2 biology and structure**

Runx2, or runt-related transcription factor 2, is a critical regulator of bone development and osteoblastic differentiation. In humans, mutations in the Runx2 gene are associated with cleidocranial dysplasia (CCD), a congenital hereditary disorder characterized by delayed ossification of midline structures, especially the collarbone and cranium.[27,28] In mice, global

deletion of Runx2 is perinatal lethal due to lack of skeletal structure.[29] During chondrogenesis, Runx2 is critical for the proliferation of early chondrocytes and hypertrophic chondrocyte formation; deletion of Runx2 in chondrocytes abolished endochondral ossification and cartilage development.[30] Besides the role in chondrocytic differentiation and maturation, Runx2 is also a well-known regulator for osteoblastic differentiation in the skeleton.[28,29] In endochondral ossification, osteoblast recruitment following hypertrophic chondrogenesis further contributes to the calcium phosphate salt deposition in bone development and remodeling.[31,32] Mechanistically, Runx2 regulates chondrocyte proliferation and maturation, as well as osteoblast differentiation, through activation of various downstream genes such as osteocalcin (OCN), osterix, alkaline phosphatase and type X collagen.[33–36]

Runx2 is a member of the RUNX family of transcriptional factors, and thus contains the key Runt DNA-binding domain, an evolutionarily conserved protein domain which is critical to its function as a developmental transcriptional factor (**Figure 1.1**). Runx2 binds directly the *cis*-acting element (osteoblast specific element 2, or OSE2) of the OCN promoter region, and regulates several other osteoblast markers in a similar manner, including alkaline phosphatase, collagen type I, bone sialoproteins, and osteopontin.[37,38] The principal Runx2 activation domain 3 (AD3) is the location of critical phosphorylation sites involved with osteoblast differentiation and mediates upstream signals.[39–41]

1.3 Role of Runx2 in vascular calcification

Although primarily associated with normal bone and cartilage development and remodeling, substantial work has alluded to the critical role of Runx2 in arterial calcification. While not normally expressed in the vasculature, Runx2 has been found to be upregulated in arteries of

patients suffering from later stages of atherosclerosis (intimal calcification) and CKD (medial calcification).[11,42] Importantly, osteogenic reprogramming of SMCs has been found to be preceded by *de novo* expression of Runx2 in aortas.[43,44] In an intimal calcification model, Runx2 expression was observed in areas of cartilaginous metaplasia prior to the development of calcification, and was considerably decreased in late-stage calcific lesions.[43]

Many studies have implicated Runx2 in osteogenic conversion and repression of smooth muscle cell phenotype, characteristics that have been well-documented in the pathogenesis of vascular calcification. Tanaka *et al.* observed that Runx2 repressed myocardin-induced activation of smooth muscle promoters (SM22α and SMMHC) and interfered with formation of the serum response factor (SRF)/myocardin complex. Knockdown of Runx2 enhanced SMC differentiation in human aortic SMCs.[45] In rat aortic SMCs, siRNA knockdown of Runx2 decreased FGF-2-induced expression of OPN, a key osteoblastic marker.[46] Likewise, previous work in our lab found that siRNA knockdown of Runx2 led to a complete blockage of phosphate-induced calcification in mouse SMCs.[47]

Several *in vivo* studies have already evaluated the effect of Runx2 on vascular calcification. Han *et al*. found that calcification induced by high doses of vitamin D_3 was completely inhibited in Runx2 truncated heterozygous mice ($Runx2^{+/\Delta C}$), and that vitamin D receptor and Runx2 are both required for vitamin D_3-induced regulation of osteogenic genes and mineral deposition.[48] Remarkably, Sun *et al.* observed that SMC-specific knockout of Runx2 in mice showed decreased high fat diet-induced calcification, decreased macrophage infiltration, and formation of osteoclast-like cells.[49] However, it should be noted that this model resulted in production of

truncated Runx2 proteins following Cre recombination, leading to potential off-target effects.[49,50] Our work directly addresses limitations of previous studies by using an improved, smooth muscle-specific targeting approach without dominant negative protein concerns.

Given the established importance of SMCs in the development of VC, we hypothesize that Runx2 in SMCs plays a critical role in promoting osteoblastic differentiation during AMC and AIC. We also hypothesize that Runx2 helps promote chondrocytic maturation during endochondral ossification and inhibits pro-healing macrophage polarization in atherosclerotic lesions. VC is an important predictor of cardiovascular mortality and these findings would further clarify Runx2's role in multiple facets of VC and could provide the basis for design of therapeutics to treat arterial calcification and atherosclerosis.

1.4 Figures

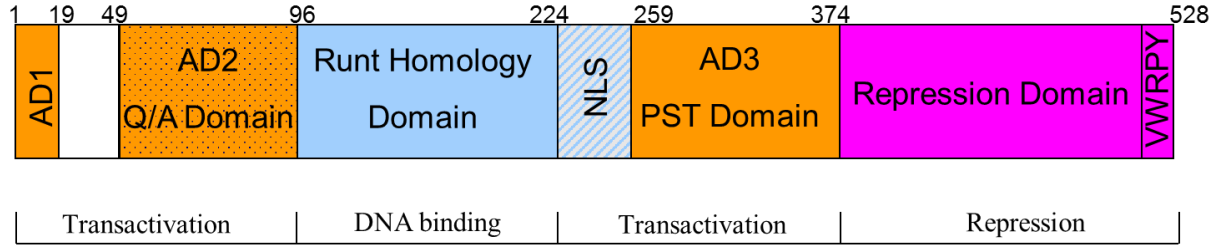

Figure 1.1: Mouse Runx2 protein structure.

Key features and functional domains include the Runt homology domain (RHD, 96-223), a nuclear localization signal (NLS, 224-258), and the AD3 domain (PST domain, 259-373). Figure adapted from Thirunavukkarasu *et al* (1998).[51]

2 Chapter 2: Determining the role of Runx2 in vascular medial calcification

2.1 Abstract

Previous work in our lab using a mouse model of medial calcification allowed us to identify vascular smooth muscle cells (SMCs) as a source for osteochondrogenic precursors and 97% of chondrocyte-like cells in calcifying vessels. Because SMCs can undergo lineage reprogramming toward osteoblastic and chondrocytic fates during VC, we propose to determine whether SMC-specific Runx2 expression is required for osteogenic phenotype change and AMC. To this end, we developed a mouse with smooth muscle-specific removal of Runx2 and induced AMC through repeated injections of vitamin D (cholecalciferol). Expression of Runx2 was indeed required for osteogenic phenotype change, as evidenced by a reduction in expression of osteoblastic markers via quantitative RT-PCR and immunohistochemical staining of Runx2$^{\Delta SM}$ aortic sections. Knockout of Runx2 also prevented development of vascular medial calcification in aortic arches and abdominal aortas. This effect was recapitulated in *in vitro* studies looking at high phosphate-induced matrix calcification of SMCs isolated from Runx2$^{\Delta SM}$ mice.

2.2 Introduction

2.2.1 Role of smooth muscle cells in vascular calcification

VC is now understood to be a highly-regulated process encompassing a variety of cardiovascular pathologies. Many different cell types have been proposed to be involved in this process, including SMCs, endothelial cells, bone marrow-derived circulating cells, macrophages, pericytes, and adventitial cells.[43,44,52–55]

Smooth muscle cells are of particular interest due to their ability to undergo lineage reprogramming toward osteoblastic and chondrocytic fates during vascular calcification.[14,44,47,56]

Previous work in our lab using a mouse model of AMC allowed us to identify vascular SMCs as a source for osteochondrogenic precursors and 97% of chondrocyte-like cells in calcifying vessels.[56] Similarly, in a follow-up studying looking at intimal calcification, over 80% of cells positive for Runx2 (an osteoblastic marker) and 98% of cells positive for Col II (a chondrocytic marker) had previously expressed SM22α, a marker for vascular SMCs.[43] These suggest that SMCs play a critical role in the development of this pathology. Thus, we propose to determine whether SMC-specific expression of Runx2 is required for osteogenic phenotype change and development of AMC.

2.3 **Materials and Methods**

2.3.1 Creation and verification of Runx2 targeting construct

As outlined in **Figure 2.1A**, a Runx2 genomic sequence (striped line) containing exon 4 (grey box) was cloned into a targeting vector. Homologous recombination (dashed line) between the targeting vector and wild type locus resulted in the targeted allele. The Neo cassette was used to select positive embryonic stem cell clones and removed from the conditional allele of chimeric mice by selective breeding onto a FLP transgenic background. Upon Cre recombination (dashed line), the resulting reading frame shift generates an early stop codon, causing production of a truncated protein and disruption of the Runt homology domain should it be translated. PCR was used to confirm the LoxP site, homologous recombination of the targeting vector and the wild type Runx2 locus, and removal of the Neo cassette in the conditional allele.

2.3.2 Generation and characterization of Runx2 global knockout mice

Two key domains of interest are either disrupted or deleted altogether in our Runx2 knockout model: the Runt homology domain is truncated while the AD3 domain is removed completely.

Our model is an improvement over existing Runx2 knockout models (which produce a truncated Runx2 protein with a functional activity) due to its ability to terminate activity from these domains, thus preventing dominant negative activity and confounding variables.

To confirm Runx2 deletion with our model, male $Runx2^{f/f}$ were crossed with female Sox2-Cre transgenic mice to produce $Runx2^{+/\Delta}$ mice. Embryos from timed inbreeding of $Runx2^{+/\Delta}$ mice were collected at 18.5 dpc (days post coitum). Subsets of $Runx2^{+/+}$, $Runx2^{+/\Delta}$, and $Runx2^{\Delta/\Delta}$ embryos were either X-rayed, double-stained for cartilage and bone with Alcian blue and Alizarin red, or fixed in 10% buffered formalin for histology.

2.3.3 Generation of smooth muscle-specific Runx2 knockout mice

$Runx2^{+/f}$ mice were further bred with SM22α-Cre transgenic mice (for smooth muscle-specific recombination of the conditional allele) (**Figure 2.1**). The 2.8-kb SM22α-Cre promoter used has previously been demonstrated and used for *in vivo* loss-of-function studies in vascular SMCs as well as genetic fate mapping studies of vascular SMCs.[43,44,57,58] Genotyping of mice was used to confirm the presence and specificity of floxed-Runx2 or recombined alleles in knockouts.

2.3.4 Vitamin D model for vascular medial calcification

In this model, AMC was induced by vitamin D_3 (cholecalciferol) overload in C57BL/6 mice.[59] Treatment with vitamin D results in increased serum calcium levels.[48] Ten-week-old $Runx2^{f/f}$ and $Runx2^{\Delta SM}$ mice received cholecalciferol subcutaneously at a dosage of 500,000 IU/kg/day for 4 consecutive days; 5% ethanol in sterile water was used as vehicle control. Animals were monitored daily and sacrificed 10-14 days post-injection with intraperitoneal injection of pentobarbital followed by exsanguination via cardiac puncture. Aortic arches and abdominal

aortas plus common iliac arteries were collected for calcium quantification, and thoracic aortas, renal arteries, and kidneys were collected for histology and quantitative RT-PCR. All protocols were in compliance with the NIH Guideline for the Care and Use of Laboratory Animals and have been approved by the Institutional Animal Care and Use Committee, University of Washington.

2.3.5 Histochemical and Immunohistochemical staining

Specimens were fixed with modified Clarke's fixative (75% methanol, 25% acetic acid, glacial) and embedded in paraffin. Serial sections at 5 μm thickness were collected and used for hematoxylin & eosin (H&E) staining. Calcium phosphate mineral was detected by Alizarin red and von Kossa staining.[44,60] Immunohistochemistry was used to determine presence of SMCs and expression of osteochondrogenic precursors. In brief, sections were deparaffinized and rehydrated, blocked for endogenous peroxidase activity and non-specific binding, and incubated with primary antibodies for SM22α (ab10135, Abcam), SMMHC (ab683, Abcam), ACTA2 (A2547, Sigma), Runx2 (MAB2006, R&D Systems) or osteopontin (AF808, R&D Systems). The presence of vascular SMCs or osteochondrogenic precursors were then visualized through biotin-conjugated secondary antibodies followed by ABC amplification (PK-6100, Vector Lab) and 3, 3'-diaminobenzidine staining (D-0426, Sigma) or through fluorescent secondary antibodies.[43,44]

2.3.6 Blood and sera analysis

For serum analysis, mice were fasted for 4 hours prior to blood collection into serum separator tubes. Sera were analyzed for cholesterol, triglyceride and phosphate levels via bioanalyzer. Calcium levels were determined using a colorimetric calcium detection kit (Teco Diagnostics,

C503-480). Blood urea nitrogen (BUN) was measured using QuantiChrom Urea Assay Kit (BioAssay System, DIUR-500).

2.3.7 Isolation and culture of primary vascular smooth muscle cells

Vascular SMCs were isolated from 4-week-old wild type (WT), $Runx2^{f/f}$, and $Runx2^{\Delta SM}$ mice. Briefly, aortas were removed from subclavian origin to diaphragmatic insertion and put into ice-cold DMEM containing antibiotic and antifungal agents. All connective tissue was removed from the aorta. Vessels were incubated with 1 mg/mL collagenase type II, 0.23 mg/mL elastase, 0.375 mg/mL soybean trypsin inhibitor, and 2 mg/mL BSA in DMEM with antibiotics and antifungal agents (0.22 µm filtered) for 3-5 minutes. Vessels were cut longitudinally, rinsed with DMEM, and pinned down with intima side up. The endothelium was removed by rolling a wetted sterilized cotton swab. The media was peeled off (from the adventitia) and cut into 3-5 mm pieces. Media pieces were placed in 0.64 mg/mL collagenase type II in 20% FBS in DMEM (0.22 µm filtered) for 20 minutes in a 37 ºC water bath. Samples were spun down, washed, and incubated in a final digestion solution of 0.64 mg/mL collagenase type II and 0.44 mg/mL elastase in 20% FBS in DMEM for 45-50 minutes in a 37 ºC water bath. The cell suspension was centrifuged at 800 x *g*, resuspended in DMEM supplemented with 20% FBS, 1% NEAA, 1% glutamine, 1% antibiotic/antifungal, and seeded into a pre-equilibrated T-25 flask. Aortic SMCs were seeded at a density of 1×10^5 cells/mL for primary culture, and split 1:2 at confluency. Cells used for the experiments were from 3rd – 9th passages. Subcultured SMCs were maintained in DMEM culture medium supplemented with 20% FBS. SMCs of over 96% purity as determined by the presence of SM22α, SMMHC and ACTA2 were used for our studies (data not shown).

2.3.8 *In vitro* calcification assay

Runx2$^{\Delta SM}$, Runx2$^{f/f}$, and Runx2$^{o/o}$ (WT) SMCs were seeded at 2.0 x 10^4 cells/well into 6-well plates. At ~70-80% confluency, cells began treatment with culture media supplemented with 2.4 mM inorganic phosphate. Media was changed every other day. Following Pi treatment of 6 or 10 days, total calcium was extracted using 0.6 N HCl and normalized to total protein (collected using 0.2 N NaOH). Calcium levels were determined using a colorimetric calcium detection kit (C503-480, Teco Diagnostics), while total protein was determined using the Pierce Micro BCA Protein Assay Kit (23225, ThermoScientific).

2.3.9 Quantification of aortic arch calcium content

Approximately 6 mm of the aortic arch from each LDLr$^{-/-}$ mouse was collected and lyophilized to a constant weight. Calcium was extracted from the lyophilized tissue with 0.6 N HCl and determined using a colorimetric calcium detection kit. Values were normalized to the dry weight of the arches.

2.3.10 DNA collection and genotyping

Genomic DNA was extracted from 3 mm tails using a DNeasy Mini Kit (69506, Qiagen). Primers used to detect Runx2 recombination/deletion were: LOX1 5' GCTCAAGACCTGACTCGAGAC 3' and NDEL2, 5' CTTGAAACCATCCACAGGTGAT 3'. Thirty cycles of PCR were used to allow exponential amplification of the desired genes, and GAPDH was used to monitor sample loading.

2.3.11 Quantitative RT-PCR

Total RNA was extracted from blood vessels or SMC monolayers using the RNeasy Mini Kit (74106, Qiagen). Contaminating genomic DNA was digested by RNase-free DNase I (79254,

Qiagen). Total RNA (0.5 – 1 μg) was used to synthesize first-strand cDNA using Omniscript (205113, Qiagen) at 37°C for 1 hour, and the cDNA produced was used to determine expression of Runx2, osteopontin (*Opn*), alkaline phosphatase (*Alpl*), and osteocalcin (*Ocn*) using Taqman quantitative RT-PCR. Primer and probe sequences are outlined in **Table 2.1**.

Probe sequences were created to span an exon-exon junction of the desired genes to avoid amplification of residual genomic DNA. In particular, Runx2 primers were generated to amplify exon 4 to determine deletion efficiency of the Runx2 conditional allele in Runx2$^{\Delta SM}$ mice. 18s ribosomal RNA expression was determined using Taqman Ribosomal RNA Control Reagents (4308329, ThermoFisher) to control sample loading. Gene expression levels were normalized to 18s ribosomal RNA levels and expressed as a fold of control samples.

2.3.12 Protein collection and western blotting

Nuclear lysates were prepared from SMC monolayers using a nuclear extraction kit (78833, Thermo Scientific). Protein content of the lysates was measured by the Pierce BCA Protein Assay Kit. Equal amounts of the protein from each sample were separated by SDS polyacrylamide gel electrophoresis (SDS-PAGE) followed by a transfer to a PVDF membrane (Perkin Elmer). Runx2 protein was then detected using an antibody specific for mouse Runx2 (D130-3, MBL Intl Corp. or sc-10758, Santa Cruz), a horseradish peroxidase-conjugated secondary antibody (Jackson ImmunoResearch Lab), and the SuperSignal West Dura Extended Duration Substrate (34075, Thermo Scientific). Probing of the same membrane with lamin B (sc-6217, Santa Cruz) was used to monitor sample loading.

2.3.13 Statistics

Data, shown as mean ± S.E.M., were analyzed with Student's t-test or one-way ANOVA with Dunn's post hoc test. Data were considered to be statistically significant at a p value < 0.05.

2.4 **Results**

2.4.1 Global deletion of Runx2

Global Runx2$^{\Delta/\Delta}$ embryos were generated by Sox2-Cre recombination of conditional Runx2 alleles. Three different amplicon sizes indicate WT (1019 bp), floxed (1219 bp) and Cre-recombined (527 bp) alleles (Figure 2.2)**.** Global Runx2$^{\Delta/\Delta}$ embryos were perinatal lethal, smaller than both Runx2$^{+/\Delta}$ and Runx2$^{\Delta/\Delta}$ embryos, and had foreshortened noses (**Figure 2.3A**). Alizarin Red S and Alcian blue staining of Runx2$^{\Delta/\Delta}$ embryos showed lack of calcified cartilage and bone development, while Runx2$^{+/+}$ embryos exhibited regular ossification (**Figure 2.3B**). Furthermore, no skeletal elements were detected in the skull, mandibles, upper and lower extremities, ribs, and vertebrae of Runx2$^{\Delta/\Delta}$ embryos (**Figure 2.3C**). No differences were observed in Runx2$^{\Delta/+}$ and Runx2$^{\Delta/\Delta}$ embryos. Defects in skeletal development of Runx2$^{\Delta/\Delta}$ embryos were similar to those in conventional targeted Runx2 knockout mice, confirming appropriate targeting of the conditional Runx2 allele.[28,29]

2.4.2 Generation and characterization of SMC-specific Runx2 knockout mice

To generate smooth muscle-specific removal of Runx2, we crossed mice with the SM22α-Cre recombinase transgenic allele onto mice with the floxed Runx2 allele (Runx2$^{f/f}$). Runx2$^{\Delta SM}$ and Runx2$^{f/f}$ were viable, normal in size, and fertile, and no differences were observed in development or immunohistological staining for SMC lineage markers. Exon 4 was efficiently deleted from aortas of Runx2$^{\Delta SM}$ mice and was absent in the aortic media (**Figure 2.4A**). In contrast, no SM22α-Cre mediated DNA rearrangement of the Runx2 gene was observed in the

liver, similar to previous observations from our lab and other investigators.[44,57,61] No developmental defects were observed in arteries of the wild type, Runx2$^{f/f}$, and Runx2$^{\Delta SM}$ mice as determined by H&E staining and IHC staining for SMC lineage markers: SM22α, SM α-actin, and SM-MHC (**Figure 2.5A-I**).

2.4.3 Deletion of Runx2 was SMC-specific and ameliorates calcification of VSMCs in culture

To determine whether the function of Runx2 in AMC was SMC-specific, we isolated vascular SMCs from aortas of wild type, Runx2$^{f/f}$ and Runx2$^{\Delta SM}$ mice and determined their calcification susceptibility in response to a calcification stimulus, inorganic phosphate. Genotypes of the SMCs were determined by genomic DNA rearrangement at exon 4 of the Runx2 gene (**Figure 2.6A**) and expression of Runx2 mRNA and protein (**Figure 2.6B-C**). SMCs isolated from Runx2$^{\Delta SM}$ mice were found to have a complete loss of Runx2 even when with elevated phosphate treatment, while Runx2$^{f/f}$ SMCs retained appropriate Runx2 response to phosphate induction. As shown in **Figure 2.7**, elevated phosphate induced matrix calcification of wild type and Runx2$^{f/f}$ SMCs in a time-dependent manner. In contrast, SMCs isolated from the Runx2$^{\Delta SM}$ mice showed significantly attenuated phosphate-induced matrix calcification compared to Runx2$^{f/f}$.

2.4.4 SMC-specific depletion of Runx2 prevents vascular calcification *in vivo*

To determine whether Runx2 expression in SMCs was required for AMC, we induced disordered mineral homeostasis in Runx2$^{f/f}$ and Runx2$^{\Delta SM}$ mice via subcutaneous injection of vitamin D_3 (VitD) at a dosage of 500,000 IU/kg/day for 4 consecutive days. VitD treatment of both Runx2$^{f/f}$ and Runx2$^{\Delta SM}$ mice led to significantly increased serum calcium, FGF23, and ALP levels compared to vehicle controls (**Figure 2.8A-C**). Serum phosphate was elevated in VitD treated

mice compared to vehicle controls, but did not achieve statistical significance, likely due to the highly elevated FGF23 in response to VitD treatment (**Figure 2.8D**).[62] BUN levels were similar in VitD- and vehicle-treated mice (**Figure 2.8E**). Furthermore, no significant differences in these serum parameters were observed between VitD treated Runx2$^{f/f}$ and Runx2$^{\Delta SM}$ animals (**Figure 2.8A-E**). Consistent with BUN findings, kidneys from VitD treated Runx2$^{f/f}$ and Runx2$^{\Delta SM}$ mice showed normal renal histology as compared to vehicle-treated Runx$^{f/f}$ mice, and lacked renal calcification. (**Figure 2.9A-C)**

In association with altered mineral homeostasis, VitD treatment rapidly induced calcification in the arteries of Runx2$^{f/f}$ mice. As shown in **Figure 2.10B**, calcification was restricted to the arterial media, highly associated with the deformed and fragmented elastic lamina (**Figure 2.10E**), and undetectable in VitD-treated Runx2$^{\Delta SM}$ vessels (**Figure 2.10C**) and vehicle control vessels (**Figure 2.10A**). Calcium content was greatly increased in aortic arches and abdominal aortas plus common iliac arteries upon VitD treatment, ranging from 4 to 12 μg/mg dry weight (Runx2$^{f/f}$ VitD, **Figure 2.10G** and **H**). Importantly, inactivation of the Runx2 gene in SMCs significantly reduced AMC by 39% in aortic arches and 79% in abdominal aortas plus common iliac arteries of Runx2$^{\Delta SM}$ mice compared to Runx2$^{f/f}$ mice. Finally, no inflammatory lesions were observed in the vasculature of VitD-treated mice (**Figure 2.10D-F**).

2.4.5 Runx2 expression in SMCs is required for Vitamin D-induced osteogenic phenotype change in mice

To determine whether Runx2 expression in SMCs was required for osteogenic phenotype transition in AMC, we performed immunohistological analysis for Runx2, SM22α, and OPN. As

expected, Runx2 was not detected in vehicle controls (**Figure 2.11A**), but expression was induced in the media after treatment with VitD in $Runx2^{f/f}$ (**Figure 2.11B**) and absent with Runx2 removal in $Runx2^{\Delta SM}$ mice (**Figure 2.11C**). In contrast, VitD treated $Runx2^{\Delta SM}$ mice showed levels of SM22α (a smooth muscle marker) equivalent to that observed in vehicle controls (**Figure 2.11D-F**). Furthermore, OPN, an osteogenic marker, was dramatically increased in the medial cells of VitD-treated $Runx2^{f/f}$ mice compared to vehicle treated controls, whereas no OPN was detectable in medial cells in VitD-treated $Runx2^{\Delta SM}$ mice (**Figure 2.11G-I**). We also quantified gene expression of *Runx2*, *Opn*, *Alpl*, and *Ocn* in these vessels via quantitative RT-PCR (**Figure 2.12A-D)**. mRNA levels of Runx2 were elevated in the VitD treated $Runx2^{f/f}$ vessels but no elevation was observed in VitD-treated $Runx2^{\Delta SM}$ vessels (**Figure 2.12A**), suggesting that SMCs are a major source of Runx2 signaling during VitD-induced VC. Finally, $Runx2^{\Delta SM}$ showed greatly reduced expression of *Opn* and completely blocked upregulation of the osteoblastic marker genes *Alpl* and *Ocn* in response to VitD (**Figure 2.12B-D**).

2.5 **Discussion**

AMC is a hallmark of aging, diabetes, and CKD, and is strongly correlated with coronary artery disease and future cardiovascular events.[7,17,18] Runx2 is a critical regulator of bone development and osteoblastic differentiation. It has been proposed as a key transcription factor controlling SMC osteogenic phenotype change and calcification in the vasculature. In this chapter, we reported the development of mice carrying an improved Runx2 conditional targeting allele for SMC-specific deletion. We demonstrated that SMC-specific Runx2 expression was required for pathological AMC development induced by VitD overload. In addition, Runx2 knockout in SMCs prevented osteogenic phenotype change. Finally, SMCs isolated from $Runx2^{\Delta SM}$ mice

lacked Runx2 protein and were unable to respond to high phosphate-induced calcification *in vitro*.

Vascular medial cells with an osteogenic phenotype are a commonly observed in AMC in both humans and animals, and are thought to be major mediators of vascular calcification.[44,60,63,64] Lineage tracing studies from our lab have confirmed that vascular SMCs can undergo lineage reprogramming and give rise to Runx2-expressing osteogenic progenitors in AMC.[44] While other groups have implicated Runx2 as a critical factor in mediating calcification of SMCs *in vitro*, our study is the first to show that SMC-specific expression of Runx2 is required for osteogenic lineage reprograming and AMC *in vivo*. In our study, VitD-treated mice developed AMC and exhibited elevated Runx2, OPN, ALP, and OCN expression and loss of SM22α expression in the tunica media. These observed changes were eliminated in $Runx2^{\Delta SM}$ mice. Furthermore, SMCs isolated from $Runx2^{\Delta SM}$ mice were much less susceptible to elevated phosphate-induced calcification than those from $Runx2^{f/f}$ and wildtype mice. Together, these findings suggest an SMC-specific role of Runx2 in AMC via control of osteogenic lineage reprogramming.

In a related study by Han *et al*. where Runx2 haploinsufficient mice were used to examine functional cooperation between vitamin D receptor and Runx2 in VitD-treated mice, they observed less AMC in $Runx2^{+/-}$ mice when treated with Vitamin D.[48] However, they also found reduced serum ALP, which may have confounded their findings due to its role in degradation of pyrophosphate, a major inhibitor of vascular calcification. Our conditional targeting strategy allowed us to selectively delete Runx2 from SMCs without affecting serum ALP levels,

osteoblast expression, or bone morphology, thereby allowing us to distinguish between skeletal and vascular effects of Runx2.

Lastly, our method for induction of vascular medial calcification (via repeated injections of Vitamin D) warrants further consideration. Patients with chronic kidney disease have traditionally been prescribed active vitamin D in an effort to lower parathyroid hormone levels. However, the effects of vitamin D may be dosage dependent, with protective effects seen at lower dosages while higher dosages stimulated aortic calcification.[65] For future studies, we would consider breeding mice with the Runx2 conditional allele onto a DBA/2 background mouse model with severe renal insufficiency and high phosphate feeding to strengthen our findings from this study.[66]

2.6 **Conclusions**

We have developed a unique mouse model to determine the role of Runx2 *in vivo* in a tissue-specific manner. We have demonstrated the importance of SMC-specific Runx2 in AMC induced by disordered mineral metabolism. Calcification was significantly reduced in both aortic arches and abdominal aortas plus iliac arteries when Runx2 was removed. Mechanistically, this effect was due to the inhibition of SMC reprogramming into osteochondrogenic progenitors. Furthermore, the effect was independent of systemic mineral homeostasis, while Runx2 deficiency in SMCs was shown to protect from matrix calcification *in vitro*. Taken together, our study revealed a critical role of Runx2 in SMC osteochondrogenic phenotype change and AMC development, and points to pathways of controlling Runx2 expression as potential therapeutic targets.

2.7 Figures

Gene		Sequence
Runx2	Forward	5’ CACCGACAGTCCCAACTTCCT 3’
	Reverse	5’ ACGGTAACCACAGTCCCATCTG 3’
	Probe	FAM—CCTTCAAGGTTGTAGCCCT—MGB 3’
Opn	Forward	5’ TGAGGTCAAAGTCTAGGAGTTTCC 3’
	Reverse	5’ TTAGACTCACCGCTCTTCATGTG 3’
	Probe	5’ FAM—TTCTGATGAACAGTATCCTG—MGB 3’
Alpl	Forward	5’ CAAGGACATCGCATATCAGCTAA 3’
	Reverse	5’ CAGTTCTGTTCTTCGGGTACATGT 3’
	Probe	5’ FAM—AGGATATCGACGTGATCAT—MGB 3’
Ocn	Forward	5’ CTGGCTGCGCTCTGTCTCT 3’
	Reverse	5’ GACATGAAGGCTTTGTCAGACTCA 3’
	Probe	5’ FAM—TGACCTCACAGATGCCAA—MGB 3’

Table 2.1: Taqman quantitative RT-PCR primer and probe sequences for osteogenic genes

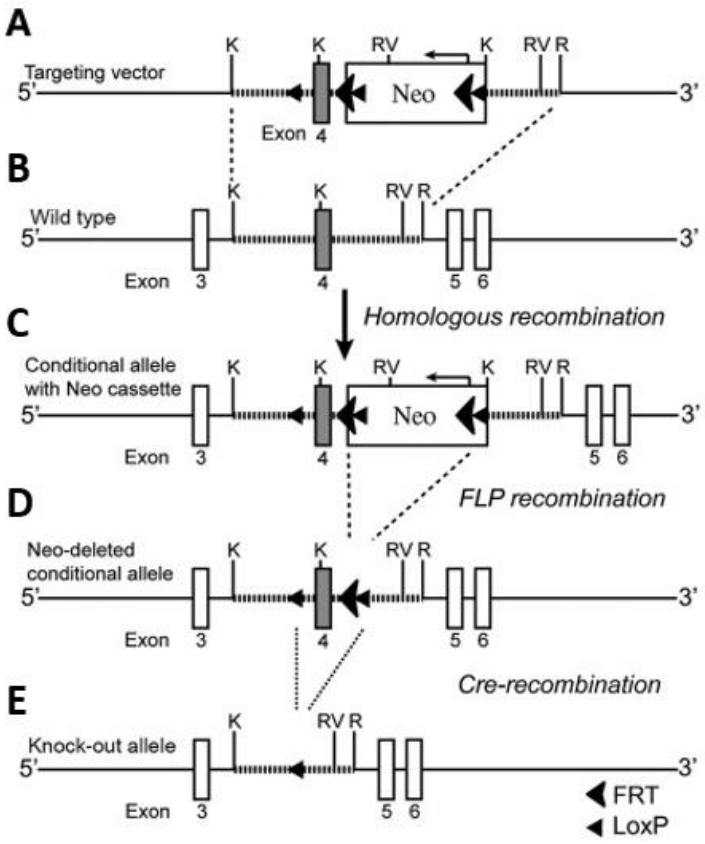

Figure 2.1: Design and characterization of a conditional Runx2 allele

Conditional targeting strategy for mouse Runx2 gene. Runx2 genomic sequence (striped line) containing exon 4 (grey box) was cloned into targeting vector **(A)**. Homologous recombination (dashed line) between targeting vector and wild type locus **(B)** resulted in the targeted allele **(C)**. The Neo cassette was used for positive selection of cells that had integrated the targeting vector into their chromosome. It was subsequently removed from the conditional allele of the chimeric mice through breeding to a FLP transgenic background **(D)**. Upon Cre recombination (dashed line), exon 4 is removed, leading to a shift in reading frame that results in a stop codon **(E)**.

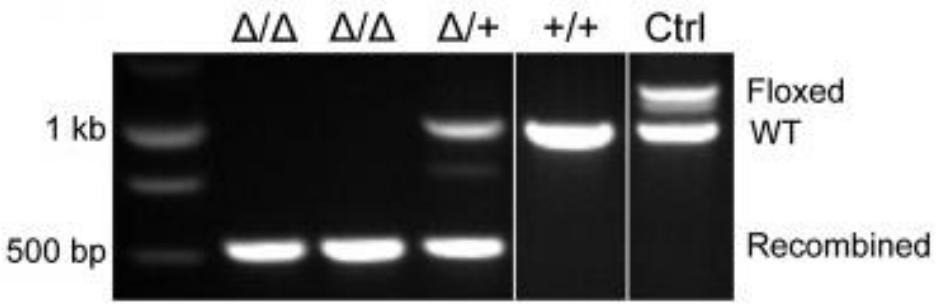

Figure 2.2: Global deletion of Runx2 was efficient.

A $Runx2^{+/flox}$ male mouse was bred to a female Sox2-Cre recombinase transgenic mouse followed by an interbreeding of the $Runx2^{+/\Delta}$ mice to generate Runx2 null mice ($Runx2^{\Delta/\Delta}$). Embryos at 18.5 dpc were genotyped. ($Runx2^{+/+}$ = wild type, $Runx2^{\Delta/\Delta}$ = knockout, and $Runx2^{+/\Delta}$ = heterozygote.)

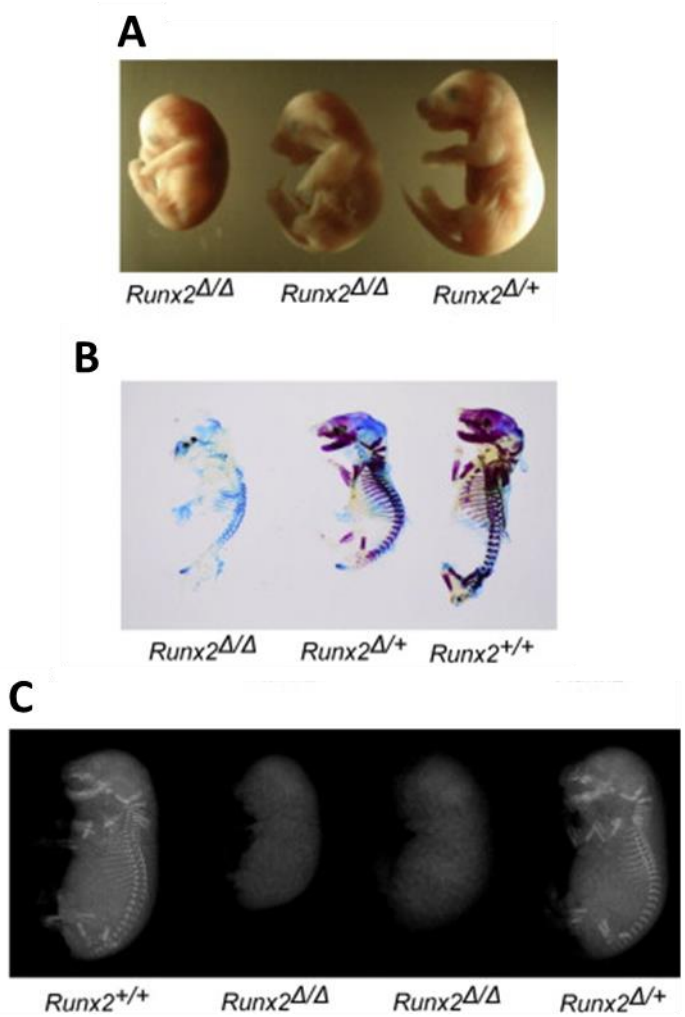

Figure 2.3: Global deletion of Runx2 leads to bone and cartilage abnormalities.

A $Runx2^{+/flox}$ male mouse was bred to a female Sox2-Cre recombinase transgenic mouse followed by an interbreeding of the $Runx2^{+/\Delta}$ mice to generate Runx2 nulls ($Runx2^{\Delta/\Delta}$). Embryos at 18.5 dpc were imaged under dissection scope (**B**). Skeletal tissues of mice with representative genotypes were determined by Alcian blue & Alizarin red stain (**C**) and by soft X-ray (**D**). ($Runx2^{+/+}$ = wild type, $Runx2^{\Delta/\Delta}$ = knockout, and $Runx2^{+/\Delta}$ = heterozygote.)

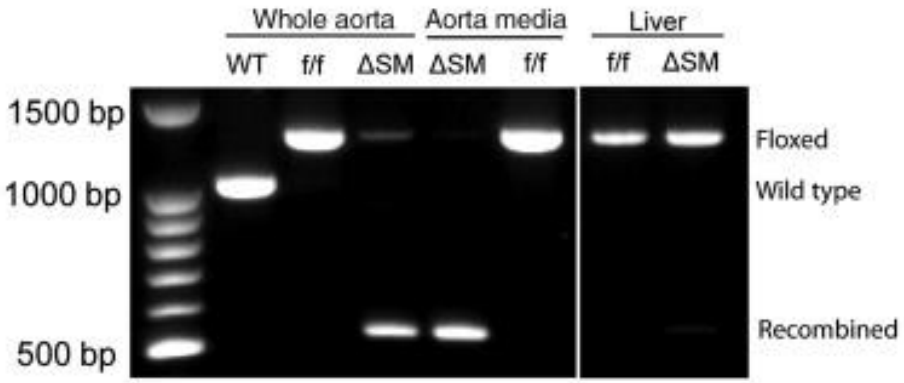

Figure 2.4: Smooth muscle-specific deletion of Runx2 was efficient.

Runx2$^{flox/flox}$ mice were bred with SM22-Cre transgenic mice to generated SMC-specific Runx2 knockout mice (Runx2$^{\Delta SM}$). Tissue-specific deletion of Runx2 was examined by PCR using primers that amplify the loxP-flanked targeting sequence. Genomic DNA from the aorta and liver were used as template. Aortic media were removed with enzymatic digestion and demonstrated a complete removal of Runx2 exon 4.

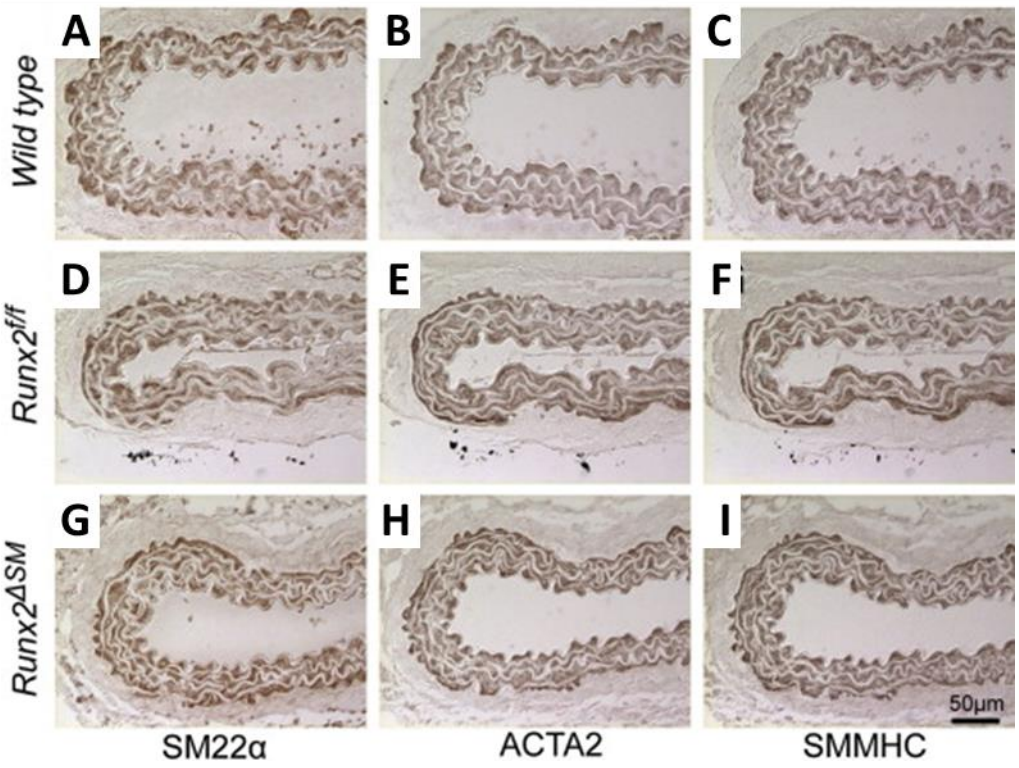

Figure 2.5: Mice with SMC-specific deletion of Runx2 show normal vascular morphology. $Runx2^{flox/flox}$ mice were bred with SM22-Cre transgenic mice to generated SMC-specific Runx2 knockout mice ($Runx2^{\Delta SM}$). Upper abdominal aortas dissected from wild type (**A-C**), $Runx2^{f/f}$ (**D-F**) and $Runx2^{\Delta SM}$ (**G-I**) mice were stained for SMC markers, SM22α (**A, D, G**), SM α-actin (ACTA2; **B, E, H**) and SMMHC (**C, F, I**).

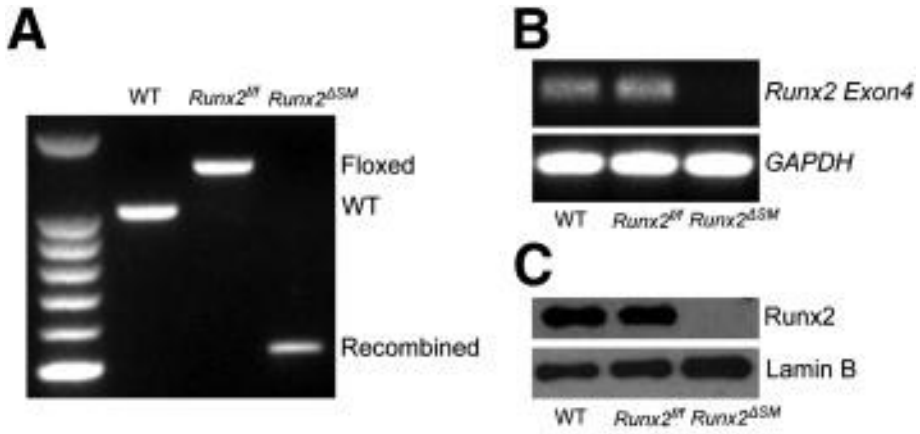

Figure 2.6: Runx2$^{\Delta SM}$ SMCs do not express Runx2.

SMCs cells were isolated from wild type (WT), Runx2$^{f/f}$, and SM22α-Cre:Runx2$^{f/f}$ (Runx2$^{\Delta SM}$) mice. Genomic DNA was extracted and the presence of WT, floxed, and knockout alleles was determined as described in Materials and Methods **(A)**. WT, Runx2$^{f/f}$, and Runx2$^{\Delta SM}$ SMCs were treated with 2.4 mM inorganic phosphate for 4 days. Total RNA and nuclear protein were extracted and used to determine the presence of exon 4 of Runx2 by RT-PCR **(B)** and Runx2 protein by Western blotting **(C)**. GAPDH and lamin B were used to monitor sample loading.

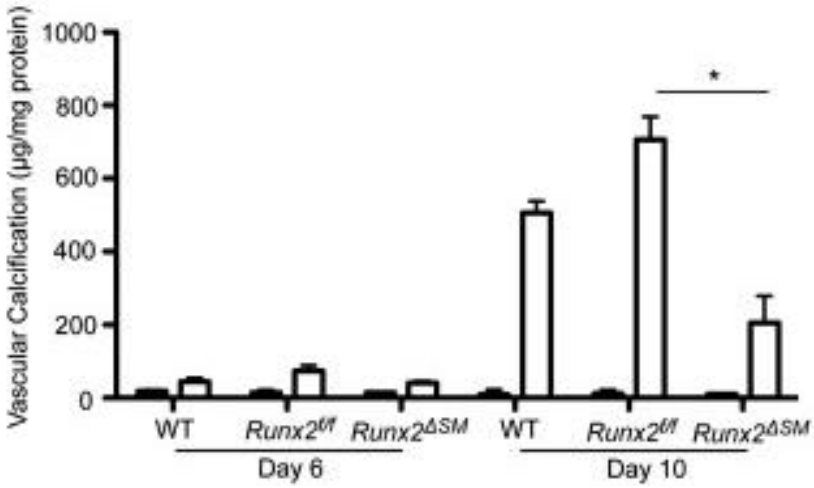

Figure 2.7: Runx2 deficient SMCs have decreased susceptibility to calcification *in vitro*. WT, Runx2$^{f/f}$, and Runx2$^{\Delta SM}$ SMCs were cultured in normal and procalcific media for 6 or 10 days. Calcium content was measured and normalized to total cellular protein. Data were presented as Mean ± S.D. (n = 3), p-value determined by one-way ANOVA with Dunn's post hoc test.

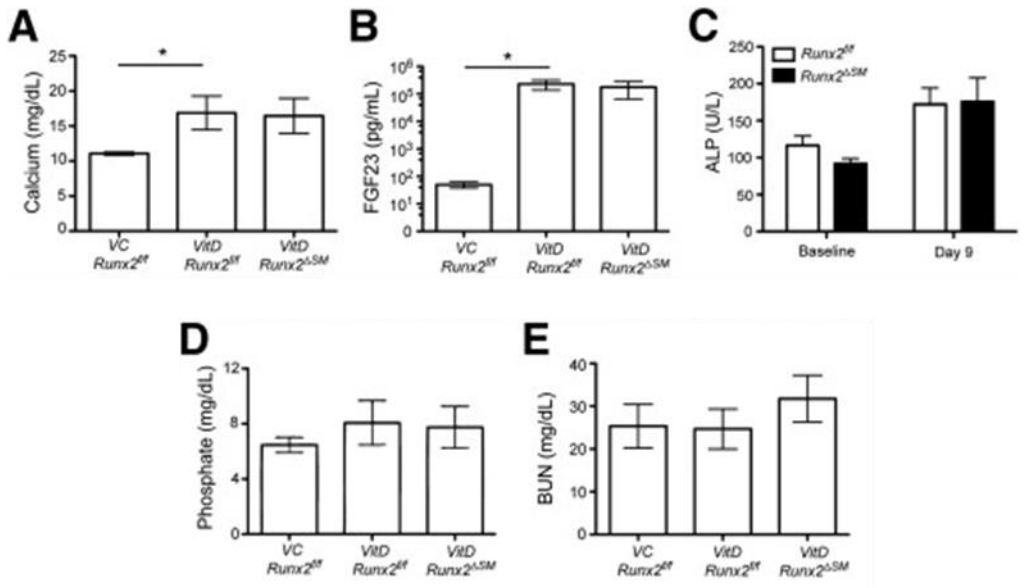

Figure 2.8: Removal of Runx2 does not affect Vitamin D-induced changes in serum calcium, FGF-23, ALP, serum phosphate, and BUN.

Vitamin D and vehicle were prepared and delivered as described in Material and Method. Fasting serum was collected from vehicle injected Runx2$^{f/f}$ and vitamin D injected Runx2$^{f/f}$ or Runx2$^{\Delta SM}$ mice. Serum calcium (**A**), FGF-23 (**B**) and ALP (**C**) levels were increased by vitamin D overload, but no differences were observed between genotypes. Serum phosphate level (**D**) and BUN level (**E**) were not significantly affected by vitamin D overload in Runx2$^{f/f}$ or Runx2$^{\Delta SM}$ mice. Data were presented as Mean ± S.D. (n = 3-5). p-value determined by one-way or two-way ANOVA with post hoc test.

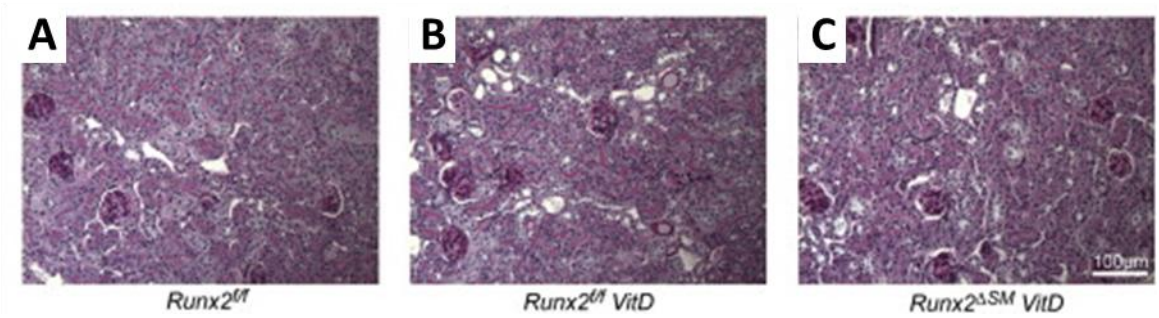

Figure 2.9: Vitamin D does not affect kidney physiology.

Vitamin D and vehicle were prepared and delivered as described in Material and Methods. Kidneys were collected from vehicle injected Runx2$^{f/f}$ and vitamin D injected Runx2$^{f/f}$ or Runx2$^{\Delta SM}$ mice. Gross kidney anatomy (Periodic acid–Schiff stain) (**A-C**) was not significantly affected by vitamin D overload.

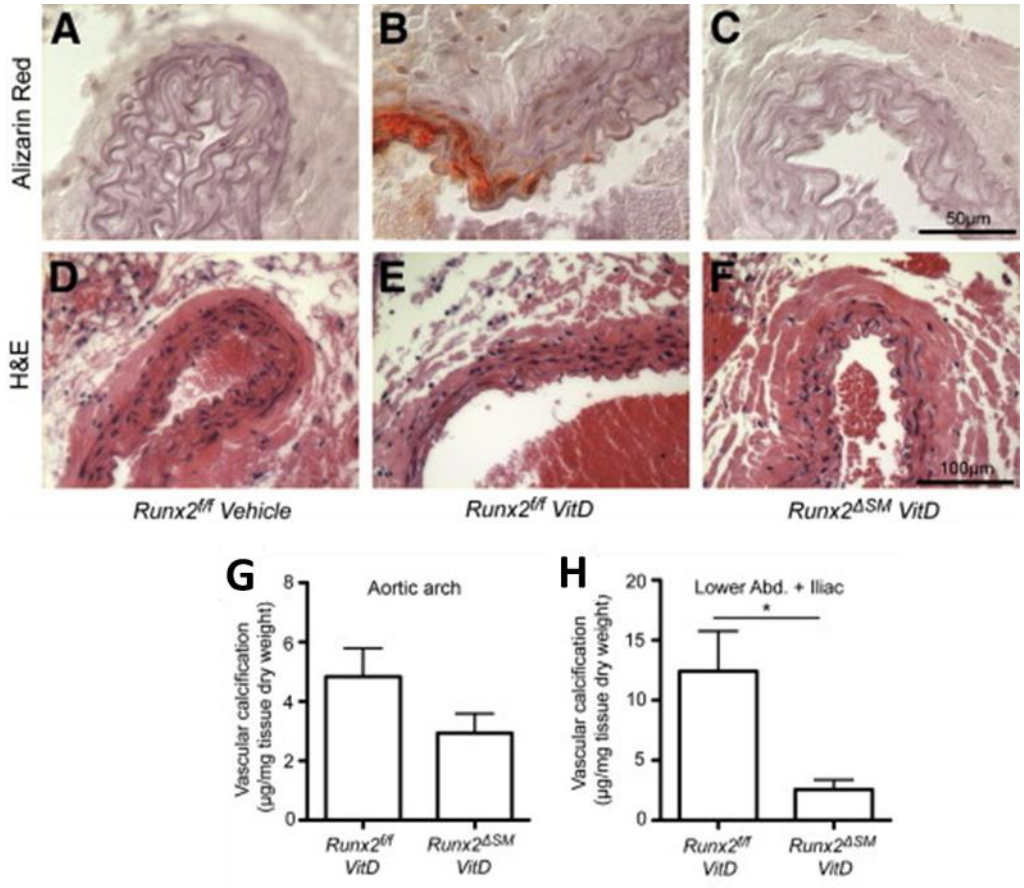

Figure 2.10: SMC-specific deletion of Runx2 prevents VitD-induced calcification.

Runx2$^{f/f}$ (**A, B, D, E**) and Runx2$^{\Delta SM}$ (**C, F**) mice were treated with either VitD (**B, C, E, F**) or vehicle control (**A, D**). Abdominal aortas were collected to visualize calcium deposition through Alizarin Red S stain (**A-C**) as well as H&E (**D-F**). Total calcium deposition in blood vessels (aortic arches or abdominal + iliac aorta) of Runx2$^{f/f}$ and Runx2$^{\Delta SM}$ mice with (VitD) treatment was quantified and normalized to tissue dry weight (**G, H**). Data were presented as Mean ± S.E.M. (*n* = 3-5). *p*-value determined by non-parametric Student t-test.

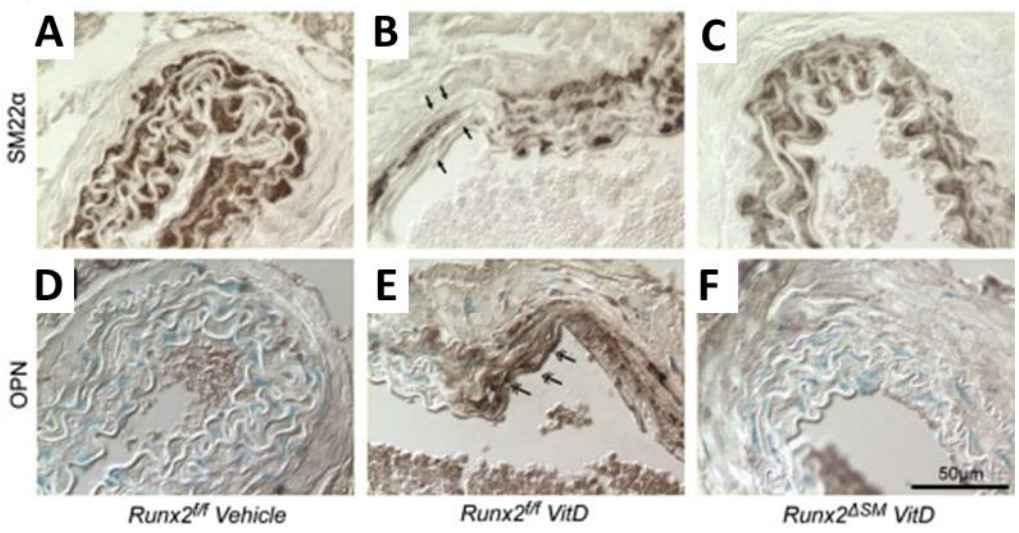

Figure 2.11: SMC-specific deletion of Runx2 prevents SMC osteochondrogenic phenotype change.

Runx2$^{f/f}$ (**A, B, D, E**) and Runx2$^{\Delta SM}$ (**C, F**) mice were treated with either VitD (**B, C, E, F**) or vehicle control (**A, D**) as described in Methods. Abdominal aortas were collected and sectioned. SMC marker protein, SM22α (**A-C**; brown stain) and osteopontin, OPN (**D-F**; brown stain).

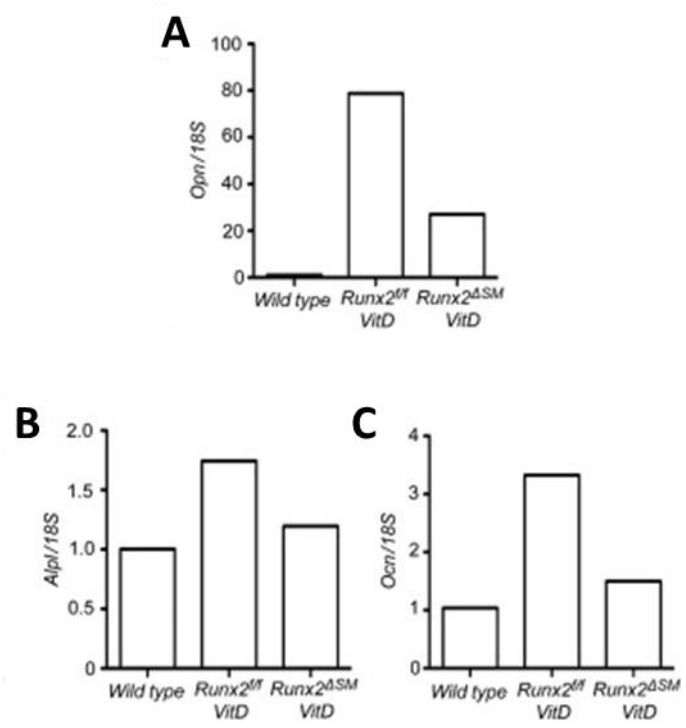

Figure 2.12: SMC-specific deletion of Runx2 inhibits osteogenic gene expression.

Total RNA was extracted from pooled thoracic aortas (n = 4) and used to determine expression of OCN, OPN and ALP by quantitative RT-PCR with 18S rRNA as internal control and untreated wild-type samples as calibrator (**A-C**).

3 Chapter 3: Determining the role of Runx2 in vascular intimal calcification

3.1 Abstract

The role of Runx2 in chondrocytic differentiation during skeletal development has been well-documented within atherosclerotic lesions. Vascular SMCs are the major cell sources contributing to chondrocytes in blood vessels. Therefore, we seek to better characterize the role of SMC-specific Runx2 expression in atherosclerosis-induced vascular calcification using an improved Runx2 conditional deletion mouse model which ensures loss of functionality of the Runt homology domain and prevents dominant negative expression. We found that Runx2 inhibited not only osteoblastic differentiation of vascular SMCs but also SMC-derived chondrocyte maturation, with its deletion leading to a 50% reduction in intimal calcification. Our studies show that while SMC expression of Runx2 was not required for initial chondrogenesis, it was necessary for maturation of chondrocytes to a pro-mineralizing, hypertrophic state associated with endochondral ossification.

3.2 Introduction

3.2.1 Runx2 and Vascular Intimal Calcification

In atherosclerosis, VC is often seen in the intimal lesion and associated with chondrocyte-like cell morphology, collagen matrices, and Runx2 expression. Previously, we demonstrated that over 80% of Runx2 positive cells in the intimal lesion were derived from SMCs.[43] Sun *et al*. further confirmed the importance of these cells using SM22α-specific Runx2 knockout mice to study atherosclerosis-induced VC.[49] In this particular study, SMC-specific Runx2 removal completely blocked VC development; this protective effect was attributed to the inhibition of macrophage infiltration and RANKL expression. However, upon Cre-mediated recombination the Runx2 targeting allele used in this study still produced a truncated Runx2 protein containing

an intact runt homology domain. This truncated Runx2 has been shown to retain DNA binding ability and can negatively affect natural Runx2 activity when introduced.[67] Another study demonstrated that their truncated Runx2 model retains partial transcriptional activity.[50] Moreover, since other runt-related transcription factors (Runx1 and Runx3) share the same vital runt DNA-binding domain, their activity could potentially be affected by the presence of transcriptionally active but functionally deficient protein. Both Runx1 and 3 are involved in regulating monocyte/macrophage biology and a truncated Runx2 protein could cause off-target effects, especially in the context of atherosclerosis, which has a major inflammatory component.[68–70] While our model addresses a similar question, we limited off-target effects on other Runx family members by ensuring loss of functionality of the Runt homology domain in the event a truncated protein is produced.

Runx2 expression has been observed in chondrocyte-like cells within the atherosclerotic lesions and its role in chondrocytic differentiation during skeletal development has been well-documented.[43,71–73] It has been suggested that Runx2 participates in both early commitment to osteochondrogenic fate as well as chondrocyte hypertrophy and maturation.[74–76] Therefore, we sought to better characterize the role of SMC-specific Runx2 expression in atherosclerosis induced vascular calcification using an improved Runx2 conditional deletion mouse model, targeting exon 4 (which codes the crucial Runt homology domain) of Runx2 directly.

3.3 Materials and Methods

3.3.1 Mouse model for vascular intimal calcification

For this model, LDLr$^{-/-}$ mice (homozygous for the Ldlr^{tm1Her} mutation) were purchased from the Jackson Laboratory (002207). These mice were crossed with mice carrying Runx2$^{f/f}$:SM22-

$Cre^{+/o}$ transgenes (as previously described) to obtain $LDLr^{-/-}$:$Runx2^{f/f}$:SM22-$Cre^{+/o}$ and $LDLr^{-/-}$:$Runx2^{f/f}$:SM22-$Cre^{o/o}$ mice, hereafter referred to as **$Runx2^{\Delta SM}$** and **$Runx2^{f/f}$** mice. These mice were fed a high fat diet (HFD; Research Diets Inc., 1.25% cholesterol, 39.9% kcal fat, 40% kcal carbohydrate) at 10 weeks of age to induce atherosclerosis, vascular cartilaginous metaplasia, and calcification, as previously described.[43] Normal chow (NC) was used as dietary control for each genotype. Body weight was recorded and fasting serum collected before the diet challenge and at termination. After 18-24 weeks of fat feeding, a total of 87 mice were euthanized via intraperitoneal injection of pentobarbital (150 mg/kg) followed by exsanguination through cardiac puncture. All protocols were in compliance with the NIH Guide for the Care and Use of Laboratory Animals and have been approved by the Institutional Animal Care and Use Committee, University of Washington.

3.3.2 Morphometric and immunohistochemical analysis of atherosclerotic vessels and cartilaginous metaplasia

To measure cartilaginous metaplasia of the lesions, eight longitudinal sections, 40 μm apart over 320 μm in depth, starting at the appearance of the three major branches on the greater curvature of the vessels were collected from each aortic arch, and 8 cross sections, 100 μm apart over 800 μm in length, starting at the bifurcation of the aortic arch, were collected from each brachiocephalic artery. Specimens were fixed with modified Clarke's fixative, processed, and embedded in paraffin.

Serial sections were made in 4 μm thickness and subject to various histochemical and immunohistochemical staining. Alizarin Red S (0.5%, pH 9.0) was used to visualize calcium

deposition. Movat pentachrome staining was used to visualize cartilaginous metaplasia. Antibodies recognizing Runx2 (MAB2006, R&D System), Sox9 (SC-20095, Santa Cruz), type II collagen (Col II; AB761, Millipore), type X collagen (Col X; LSL-LB-0092, Cosmo Bio Co., LTD.), and osteocalcin (OCN; SC-30045, Santa Cruz) were used to detect osteochondrogenic precursors, prechondroblasts, chondrocytes, and osteoblasts immunohistochemically. Signals were amplified through biotinylated secondary antibodies and Vectastain ABC Elite kit (PK-6100, Vector Lab), and visualized with 3, 3'-diaminobenzidine peroxidase substrate (D-0426, Sigma). All IHC staining was validated with non-specific IgG controls as well as negative and positive control tissues.

Cartilaginous metaplasia was identified by yellow (collagen rich) and blue (proteoglycan rich) stain consisting of chondrocyte-like cells, and expressed as percent intimal area. To assess chondrocytic differentiation in aortic arches, Sox9 positive cells and collagen type II and X positive matrices were determined immunohistochemically using the same sampling scheme. Sox9 positive cells were determined as percentage of total intimal cells. Collagen type II and X positive matrices were scored as percentage of cartilaginous metaplasia (0%, 10%, 25%, 50% and 75%) blindly and independently by two investigators, and expressed as Col X to Col II ratio using adjacent sections.

3.3.3 Quantitative RT-PCR

Total RNA was extracted from aortic arches and used to synthesize first-strand cDNA using Omniscript at 37°C for 1 hour. The cDNA produced was used to determine expression of osteochondrogenic transcription factor (Runx2), chondrogenic transcription factor (Sox9), chondrocyte marker gene (COL2A1), hypertrophic chondrocyte marker genes (COL10A1 and

MMP13), and osteoblast marker genes (osterix (OSX), alkaline phosphatase (ALP) and OCN) using Taqman quantitative RT-PCR. We also determined genes associated with macrophage recruitment, including monocyte chemotactic protein 1 (MCP1), C-C chemokine receptor type 2 (CCR2), and receptor activator of nuclear factor kappa-B ligand (RANKL) quantitatively. Primer and probe sequences are outlined in **Table 2.1** and **Table 3.1**. Primers/probes of *Col X* (Mm00487041_m1), *MMP13* (Mm00439491_m1), *MCP1* (Mm00441242_m1), *CCR2* (Mm00438270_m1), and *RANKL* (Mm00441906_m1) were purchased from Life Technologies.

All the probe sequences span an exon-exon junction of the desired genes to avoid amplification of residual genomic DNA. In particular, Runx2 primers were generated to amplify exon 4 to determine deletion efficiency of the Runx2 conditional allele in Runx2$^{\Delta SM}$ mice. 18s ribosomal RNA expression was determined using Taqman Ribosomal RNA Control Reagents (ABI) to control sample loading. Gene expression levels were determined in triplicates, normalized to 18s ribosomal RNA levels, and expressed as a fold of control samples.

3.3.4 Statistics

Normality of distribution was assessed with D'Agostino-Pearson normality test. Normally distributed data are shown as means ± S.E.M., and were analyzed with Student's t-test for comparison of 2 groups and two-way ANOVA and Bonferroni's post hoc test for comparison of multiple groups. Non-normally distributed data were analyzed with Student's t-test. Data are considered statistically significant at a p value < 0.05.

3.4 **Results**

3.4.1 Runx2 deletion in SMCs does not alter blood cell counts, serum lipid or mineral profiles

Similar to Runx2$^{\Delta SM}$ mice used in **Chapter 2**, SM22α-Cre-directed removal of Runx2 in blood vessels of LDLr$^{-/-}$:Runx2$^{\Delta SM}$ mice was efficient. As shown in **Figure 3.1**, Runx2 removal was efficient in aortas of the Runx2$^{\Delta SM}$ mice and was completely deleted in the aortic media compared to the Runx2$^{f/f}$ mice. In contrast, no SM22α-Cre mediated DNA rearrangement of the Runx2 gene was observed in the liver of the Runx2$^{\Delta SM}$ mice. Removal of Runx2 in SMCs did not affect blood counts, including white blood cells, red blood cells, hemoglobin, hematocrit, mean corpuscular volume and hemoglobin, and platelets (data not shown). Feeding with HFD induced significant hypertriglyceridemia and hypercholesterolemia in both genotypes compared to normal chow (NC) fed mice (**Table 3.2**). No significant differences in serum calcium and phosphate levels were observed between HFD and NC groups for either genotype. BUN levels were slightly elevated in Runx2$^{\Delta SM}$ mice in comparison to Runx2$^{f/f}$ mice, but were well within the reported normal range.[43] These data suggest that removal of Runx2 in SMCs does not affect systematic lipid metabolism or mineral homeostasis in LDLr$^{-/-}$ mice.

3.4.2 Characterization of SMC-specific Runx2 knockout mice on LDLr$^{-/-}$ background

In **Chapter 2**, we outlined VSMC-specific removal of Runx2 in our newly created Runx2$^{\Delta SM}$ mouse model. These mice, when bred onto an atherogenic LDLr$^{-/-}$ background and fed with a NC diet, showed normal arterial morphology, and no Runx2-positive cells were detected in either Runx2$^{f/f}$ or Runx2$^{\Delta SM}$ vessels (**Figure 3.2A**). HFD feeding induced atherosclerotic lesion formation (**Figure 3.3A**) in Runx2$^{f/f}$ mice arteries, with abundant Runx2 positive cells found throughout the lesions and in medial cells underlying the lesions (**Figure 3.2B**). Consistent with

our previous genetic fate mapping studies, most Runx2 positive cells lost their original lineage identity, as determined by dual fluorescent immunohistochemistry for Runx2 and SM22α.[43] While comparable intimal lesions also formed in the arteries of HFD fed Runx2$^{\Delta SM}$ mice (**Figure 3.3B**), removal of Runx2 in vascular SMCs dramatically reduced the number of Runx2 positive cells (**Figure 3.2C**), notably in the deep intima and the inner layers of media underneath atherosclerotic lesions, areas where osteochondrogenic differentiation of vascular SMCs starts.[43] Quantitation of Runx2 mRNA levels gave similar results between genotypes. As shown in **Figure 3.2D**, HFD induced Runx2 mRNA levels in the aortic arch by over two-fold compared to NC mice. SMC-specific Runx2 knockout led to an 87% reduction of Runx2 mRNA levels in NC vessels and 69% reduction in HFD vessels.

3.4.3 Runx2 is required for development of arterial intimal calcification

Atherosclerotic lesions in both Runx2$^{f/f}$ and Runx2$^{\Delta SM}$ vessels contained AIC as measured by Alizarin Red S staining (**Figure 3.4A** and **B**). These mineral deposits were predominantly co-localized to regions containing cartilaginous metaplasia (**Figure 3.4C** and **D**). AIC was quantitated using aortic arches collected from Runx2$^{f/f}$ and Runx2$^{\Delta SM}$ mice following 24 weeks of HFD diet challenge. Removal of Runx2 in vascular SMCs resulted in a 50% reduction of calcium deposition in atherosclerotic intima of Runx2$^{\Delta SM}$ vessels (**Figure 3.5A**).

Since calcification was predominantly co-localized to areas of cartilaginous metaplasia, we proposed that a reduction in chondrogenic differentiation of SMCs might explain the decreased calcification observed in Runx2$^{\Delta SM}$ compared to Runx2$^{f/f}$ mice. However, quantitation of Movat pentachrome-stained specimens indicated that removal of Runx2 in SMCs did not alter the lesion

fraction of cartilaginous metaplasia in Runx2$^{\Delta SM}$ vessels in comparison to the Runx2$^{f/f}$ counterparts (**Figure 3.5B**).

3.4.4 Runx2 deletion inhibits chondrocytic maturation of SMCs, but does not affect early chondrogenesis

To determine whether SMC-specific removal of Runx2 might instead affect specific stages of chondrocyte differentiation and in so doing prevent AIC progression, we determined expression levels of major chondrocytic differentiation marker genes in aortas: Sox9 (a master transcription factor critical for prechondrogenic fate decision), Col II (a marker for proliferating chondrocytes at an early differentiation state), and Col X and MMP13 (markers for mature, hypertrophic chondrocytes).[71,77,78]

Sox9 and Col II mRNA levels were elevated to similar extents in aortic arches of both Runx2$^{f/f}$ and Runx2$^{\Delta SM}$ mice in response to HFD challenge (**Figure 3.6A** and **Figure 3.7A**). In contrast, Col X and MMP13 mRNA levels were greatly reduced in Runx2$^{\Delta SM}$ mice compared to Runx2$^{f/f}$, with the drop in MMP13 expression being statistically significant ($p < 0.05$) (**Figure 3.8A** and **Figure 3.9**). Similarly, immunohistochemical staining and quantification found that levels of Sox9-positive cells (**Figure 3.6B-D**) and Col II-positive matrices (**Figure 3.7B-C**) were not altered by SMC-specific Runx2 deletion suggesting that the initial commitment of SMC to chondrocyte differentiation in calcifying blood vessels was largely unaffected by Runx2 deficiency. Similar to our mRNA findings, Col X protein expression was greatly reduced in Runx2$^{\Delta SM}$ vessels compared to Runx2$^{f/f}$ vessels (**Figure 3.8B** and **C**). Further morphometric analysis of Col II and Col X in cartilaginous matrices from adjacent sections confirmed a

reduced Col X/II ratio (**Figure 3.10**), suggesting a critical role of Runx2 in maturation of SMC-derived chondrocytes to hypertrophic chondrocytes.

3.4.5 Runx2 deletion blocks osteoblastic differentiation in atherosclerotic blood vessels

In addition to its role in chondrocytic differentiation and maturation, Runx2 is also a well-known regulator for osteoblastic differentiation in bone development.[28,29] To determine whether Runx2 was required for osteogenic differentiation of SMCs in atherosclerotic blood vessels, we determined levels of osteoblast marker genes: OSX, ALP, and OCN. Expression of OSX and ALP was substantially induced by HFD in $Runx2^{f/f}$ mice (**Figure 3.11A-B**). Removal of Runx2 in vascular SMCs of HFD-fed mice reduced OSX and ALP expression by over 55%. Similarly, expression of OCN was much higher in vessels from HFD fed $Runx2^{f/f}$ mice compared to $Runx2^{\Delta SM}$ mice (**Figure 3.11C**), and immunohistochemical staining confirmed a significant reduction in expression in $Runx2^{\Delta SM}$ vessels compared to $Runx2^{f/f}$ (**Figure 3.12**). These findings identified an essential role of Runx2 in SMC transdifferentiation to osteogenic progenitors and osteoblasts during AIC.

3.4.6 Runx2 deletion partially rescues smooth muscle marker expression

Upregulation of osteoblastic gene expression in SMCs is usually accompanied by a decrease in smooth muscle marker expression, and is associated with smooth muscle phenotype transition.[56] To determine whether an atherogenic diet decreases smooth muscle marker expression, we measured levels of smooth muscle marker genes: SM22α and SMMHC (**Figure 3.13**). Both HFD-fed $Runx2^{f/f}$ and $Runx2^{\Delta SM}$ expressed much lower expression of smooth muscle markers, while removal of Runx2 partially rescues their expression. This effect was HFD-dependent and not observed in NC-fed mice.

3.5 **Discussion**

In this chapter, we utilized an improved conditional Runx2 knockout mouse model to investigate the role of SMC-specific Runx2 in atherosclerotic vascular calcification. We developed a mouse model that targets exon 4 of the Runx2 gene and hence no functional Runx2 protein could be produced upon Cre-mediated gene deletion.[79] After introduction of this transgene into atherosclerotic $LDLr^{-/-}$ mice, we found that SMC-specific removal of Runx2 inhibited not only osteoblastic differentiation of vascular SMCs but also SMC-derived chondrocyte maturation, leading to a 50% reduction of AIC.

We observed a substantial decrease in expression of key osteogenic genes, including osterix, alkaline phosphatase, and osteocalcin in calcifying atherosclerotic vessels following SMC-specific Runx2 deletion (**Figure 3.11** and **Figure 3.12**). These findings are consistent with Runx2's role in skeletal development, where it acts as a critical transcriptional factor in the development and maturation of osteoblasts leading to intramembranous ossification and bone formation.[28,29] Accordingly, removal of Runx2 also partially rescued smooth muscle marker expression, though not completely, suggesting advanced osteochondrogenic differentiation of SMCs. In cardiovasculature, Runx2 and its downstream genes have long been found in cells surrounding mineral nodules of human and animal AMC.[11,14,56,80] Through a genetic fate mapping strategy, these cells were identified as transdifferentiated SMCs on their way to an osteoblastic fate prior to matrix calcification.[44] Deletion of Runx2 in vascular SMCs, therefore, prohibits osteoblastic differentiation and AMC, consistent with the current findings of osteoblastic differentiation in AIC.[79]

Given previous studies suggesting a role for Runx2 in chondrogenic differentiation of SMCs *in vitro* and *in vivo*, we were surprised that deletion of Runx2 in SMCs did not change the overall content of chondrocyte-like cells in the intima.[43,44,47,49,81] Our studies show that while SMC expression of Runx2 was not required for initial chondrogenesis, it was necessary for maturation of chondrocytes to a pro-mineralizing, hypertrophic state, leading to endochondral ossification. Runx2 expression has been observed in chondrocyte-like cells within atherosclerotic lesions and its role in chondrocytic differentiation during skeletal development has been well-documented.[43,71–73] Initial chondrocyte differentiation through Sox9, a master chondrogenic transcriptional factor, is absolutely critical and has been shown to act upstream of Runx2, suggesting Runx2-independent mechanisms during early-stage chondrogenesis.[82,83] In a Runx2 global knockout mouse model, isolated chondrocytes proliferated normally but were unable to maintain chondrocyte phenotype in culture.[72] Similarly, in our study, we found that Runx2 was not required for SMC-specific chondrocyte differentiation, suggesting a Runx2-independent mechanism for initial chondrocyte commitment. Other factors (including Sox9) may play a role in Runx2-independent chondrocyte differentiation, although additional work is necessary to clearly identify these factors.[84] Lastly, removal of Runx2 resulted in attenuated expression of both type X collagen and MMP13, markers signifying the terminal stage of chondrocyte differentiation and strongly associated with endochondral ossification. This restraint in chondrocyte maturation thus represents a plausible mechanism for the AIC protection seen in Runx2$^{\Delta SM}$ mice, even as cartilaginous lesion size remained unchanged in these vessels (**Figure 4.2** and **Figure 4.3).** Taken together, our data support the hypothesis that SMC-specific removal of Runx2 prevents both endochondral and intramembranous ossification in atherosclerotic lesions.

Lastly, we observed a population of Runx2 positive cells present at the outer intimal lesion of $Runx2^{\Delta SM}$ vessels. Taken together with our findings indicating 35% residual expression of Runx2 mRNA in the conditional knockout vasculature, these data suggest compensation for Runx2 removal by non-SM22 expressing cells, which may include endothelial cells, circulating bone-marrow derived cells, and pluripotent stem cells. Intriguingly, partial expression of SM22α-Cre in the circulating monocyte population may also contribute to the protective effect seen in our study. It is thus of significant interest to determine the origin of these cells to further clarify the effect of SM-specific Runx2 targeting in atherosclerotic vascular calcification.

3.6 Conclusions

We have demonstrated that SMC-specific Runx2 plays critical roles in both osteoblastic differentiation and chondrocytic maturation during atherosclerotic vascular calcification, and its deletion resulted in a 50% reduction of AIC. This protective effect was independent of systemic lipid metabolism, mineral balance, and initial chondrogenesis. Given its role, targeting the Runx2 signaling pathway in the vasculature may provide a novel therapeutic pathway for prevention of this disease.

3.7 Figures

Gene		Sequence
Sox9	Forward	5’ GCGGAGCTCAGCAAGACTCT 3’
	Reverse	5’ GGTGGTCTTTCTTGTGCTGCA 3’
	Probe	FAM-TCTGGAGGCTGCTGAA-MGB
Col2a1	Forward	5’ GGCAACAGCAGGTTCACATACA 3’
	Reverse	5’ CTTCTGTGATCGGTACTCGATGAC 3’
	Probe	5’ FAM-TGGCTGCACGAAACA-MGB 3’
Osx	Forward	5’ GGTTCTCTCCATCTGCCTGACT 3’
	Reverse	5’ CAGGGGACTGGAGCCATAGT 3’
	Probe	5’ FAM-CTGCTTGAGGAAGAAG-MGB 3’

Table 3.1: Taqman quantitative RT-PCR primer and probe sequences for osteochondrogenic genes

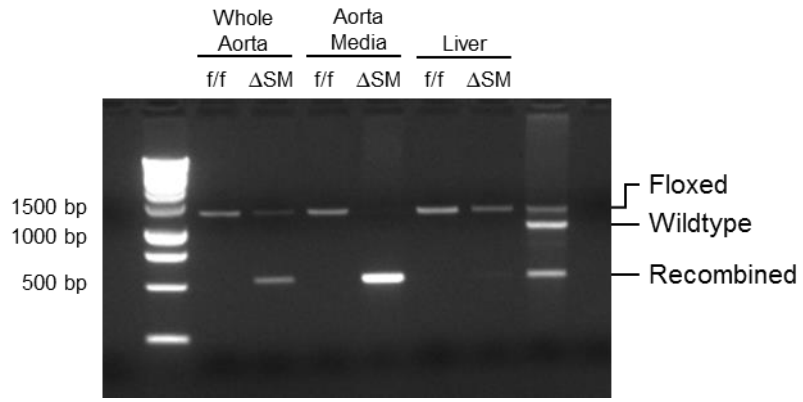

Figure 3.1: Smooth muscle-specific deletion of Runx2 was efficient in LDLr-/- mice.

Tissue-specific deletion of Runx2 was determined by PCR using primers that amplify the loxP-flanked targeting sequence. Genomic DNA isolated from aorta, aortic media, and liver of LDLr$^{-/-}$:Runx2$^{f/f}$ (f/f) and LDLr$^{-/-}$:Runx2$^{\Delta SM}$ (ΔSM) mice was used as a template.

	Normal Chow		High Fat Diet	
	LDL$^{-/-}$:Runx2$^{f/f}$	LDLr$^{-/-}$:Runx2$^{\Delta SM}$	LDL$^{-/-}$:Runx2$^{f/f}$	LDLr$^{-/-}$:Runx2$^{\Delta SM}$
Triglyceride (mmol/L)	0.65 ± 0.06	0.79 ± 0.05	7.08 ± 1.40 *	4.96 ± 0.79 *
Cholesterol (mmol/L)	6.26 ± 0.42	5.95 ± 0.36	42.74 ± 2.83 *	36.50 ± 1.90 *
Phosphate (mmol/L)	0.91 ± 0.05	1.07 ± 0.05	0.87 ± 0.07	1.00 ± 0.06
Calcium (mmol/L)	2.62 ± 0.14	2.57 ± 0.02	2.57 ± 0.06	2.58 ± 0.04
BUN (mmol/L)	13.67 ± 0.45	15.62 ± 0.74 †	11.57 ± 0.78	14.16 ± 0.51 †

Data represented as Mean ± S.E.M., N = 8 – 12, and analyzed by two-way ANOVA.
*P < 0.0001 (*vs* normal chow), † P < 0.05 (vs LDL$^{-/-}$:Runx2$^{f/f}$).

Table 3.2: Blood chemistry of Runx2$^{f/f}$ and Runx2$^{\Delta SM}$ mice fed with HFD or NC for 24 weeks.

HFD induced significant hypertriglyceridemia and hypercholesterolemia. Phosphate, calcium, and BUN were not affected.

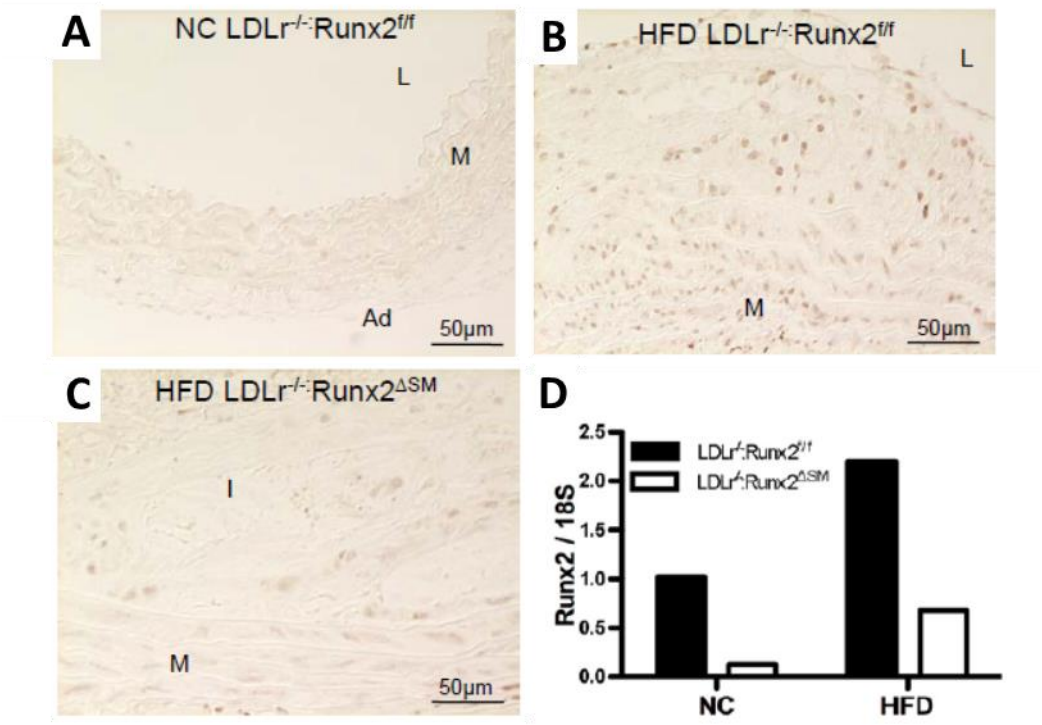

Figure 3.2: SM-specific removal of Runx2 in vascular SMCs in LDLr$^{-/-}$ mice.

Runx2$^{f/f}$ and Runx2$^{\Delta SM}$ mice were fed with normal chow (**A**) or HFD (**B** and **C**) for 18 weeks. **D**. Total RNA was extracted from pooled 18-week aortic arches and used to determine expression of Runx2 by Taqman quantitative RT-PCR (n = 5–7).

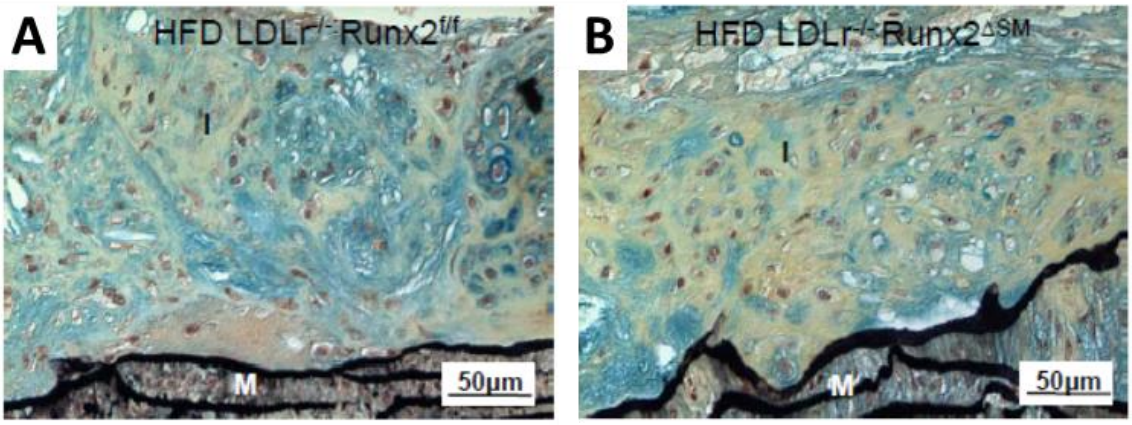

Figure 3.3: HFD induces atherosclerosis and cartilaginous metaplasia in vessels of LDLr$^{-/-}$ mice.

LDLr$^{-/-}$:Runx2$^{f/f}$ and LDLr$^{-/-}$:Runx2$^{\Delta SM}$ mice (**A** and **B**) were fed with HFD for 18 weeks. Aortic arches were collected for Movat pentachrome staining (*yellow* = collagen rich, *blue* = proteoglycan rich).

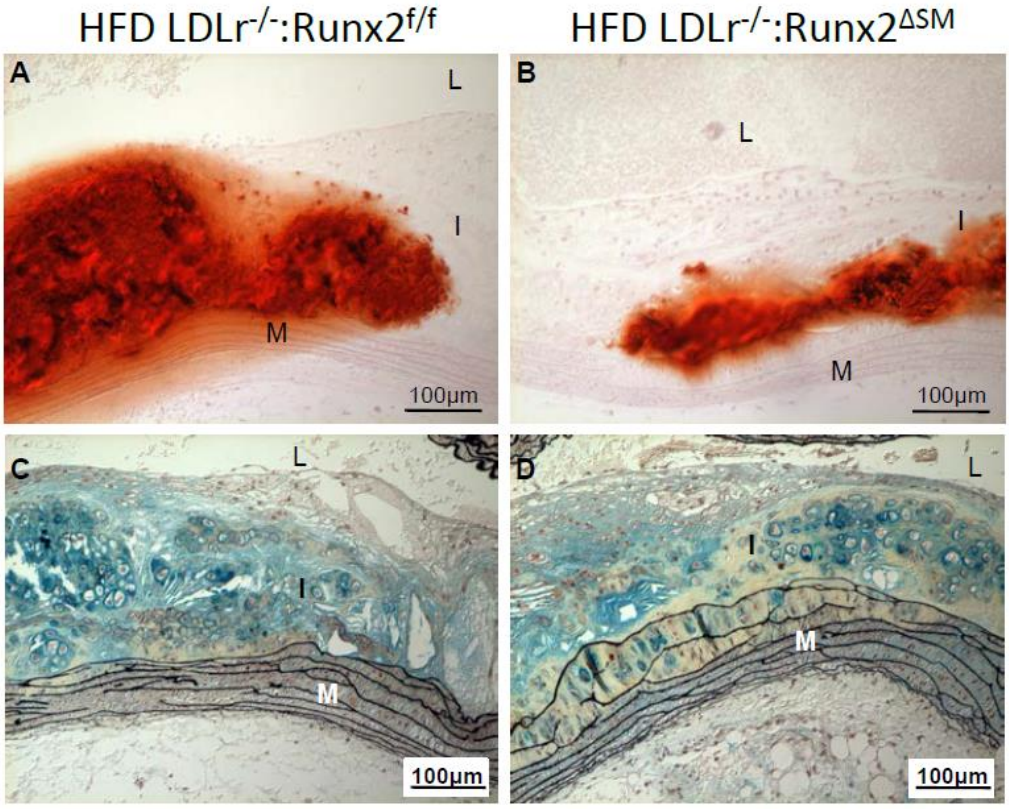

Figure 3.4: Alizarin Red S and Movat pentachrome staining of AIC in LDLr$^{-/-}$ mice.

LDLr$^{-/-}$:Runx2$^{f/f}$ and LDLr$^{-/-}$:Runx2$^{\Delta SM}$ mice were fed with normal chow (NC) or high fat diet (HFD) for 24 weeks. Aortic arches were collected for Alizarin Red S staining of mineral (**A** and **B**; red), Movat pentachrome staining (**C** and **D**; *yellow* = collagen rich, *blue* = proteoglycan rich).

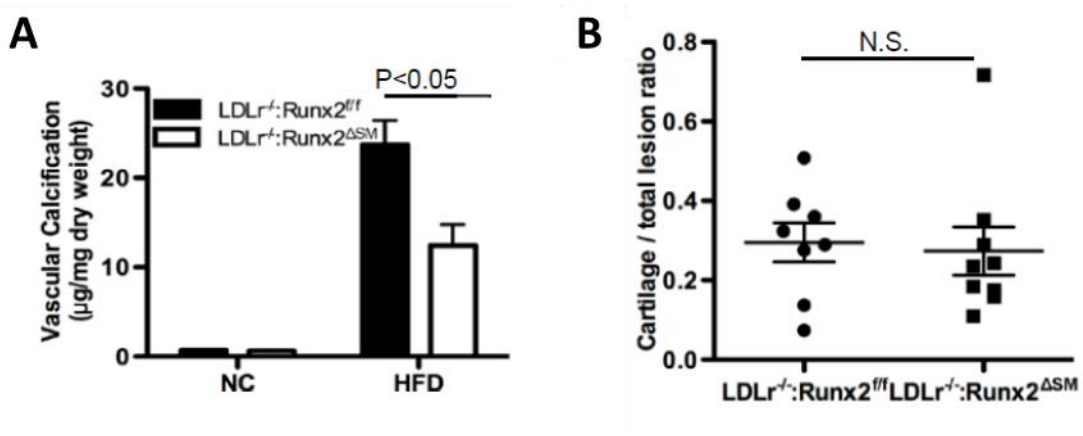

Figure 3.5: Removal of Runx2 in SMCs reduces AIC in LDLr$^{-/-}$ mice fed with HFD diet. LDLr$^{-/-}$:Runx2$^{f/f}$ and LDLr$^{-/-}$:Runx2$^{\Delta SM}$ mice were fed with normal chow (NC) or high fat diet (HFD) for 24 weeks. Aortic arches were collected for colorimetrical quantification of the arch calcium amounts (**A**, n = 10–12). Movat pentachrome-stained sections of HFD arches were also used to quantify intimal cartilaginous metaplasia morphometrically (**B**, n = 8 – 9). Data shown are Mean ± S.E.M.

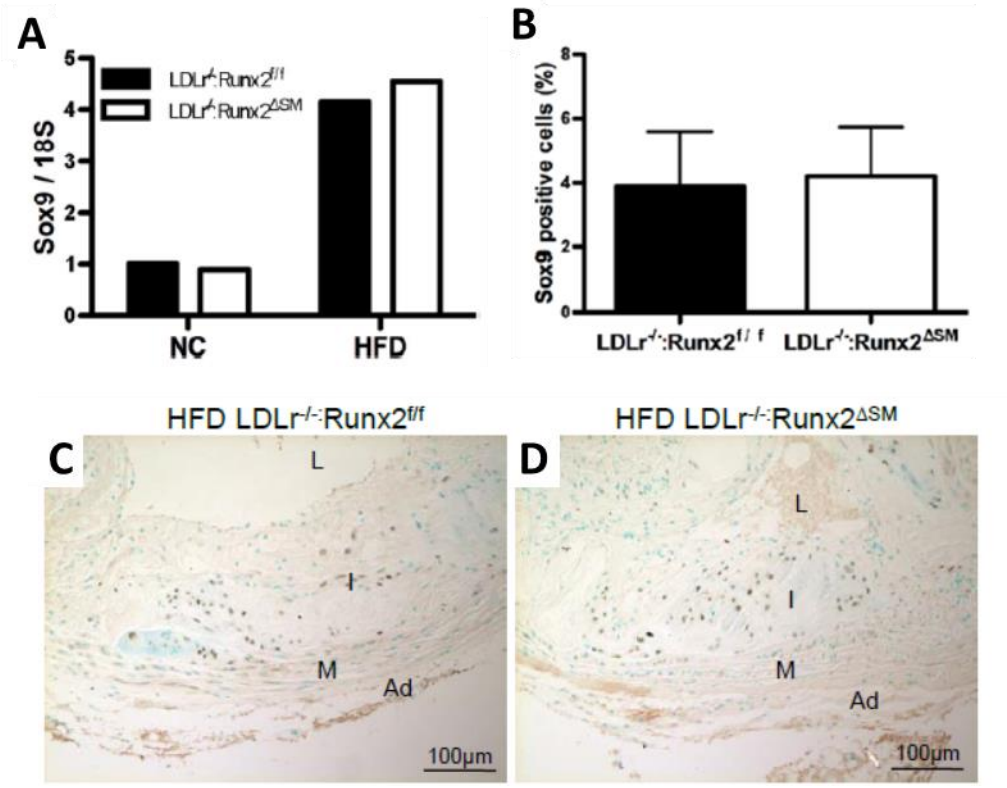

Figure 3.6: Sox9 expression was unchanged in Runx2$^{\Delta SM}$ mice.

LDLr$^{-/-}$:Runx2$^{f/f}$ and LDLr$^{-/-}$:Runx2$^{\Delta SM}$ mice were fed with normal chow (NC) or high fat diet (HFD) for 18 **(A)** and 24 weeks **(B**–**D)**. 18-week aortic arches were pooled for RNA extraction and quantitative RT-PCR of Sox9 (n = 5 – 7). Data shown are one of the two RNA preparations. 24-week aortic arches were collected from HFD animals for immunohistochemical staining (brown) of Sox9 **(C** and **D).** Data shown are Mean ± S.E.M.

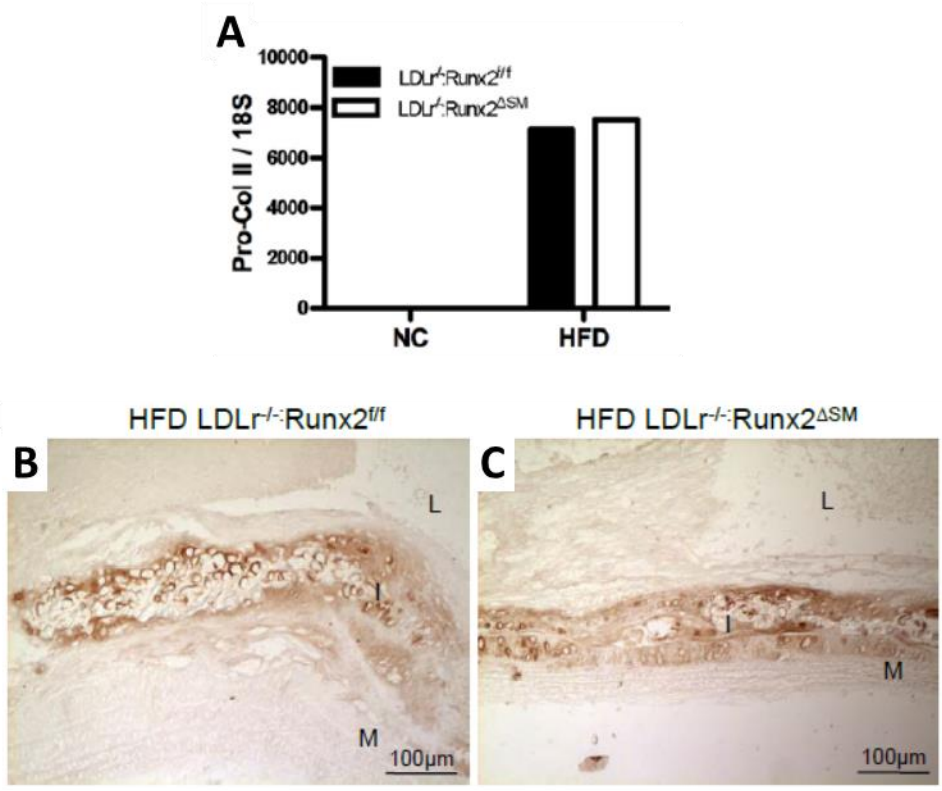

Figure 3.7: Col II expression was unchanged in Runx2$^{\Delta SM}$ mice.

LDLr$^{-/-}$:Runx2$^{f/f}$ and LDLr$^{-/-}$:Runx2$^{\Delta SM}$ mice were fed with normal chow (NC) or high fat diet (HFD) for 18 **(A)** and 24 weeks **(B** and **C)**. 18-week aortic arches were pooled for RNA extraction and quantitative RT-PCR of Col II (n = 5 – 7). Data shown are one of the two RNA preparations. 24-week aortic arches were collected from HFD animals for immunohistochemical staining (brown) of Col II **(B** and **C).**

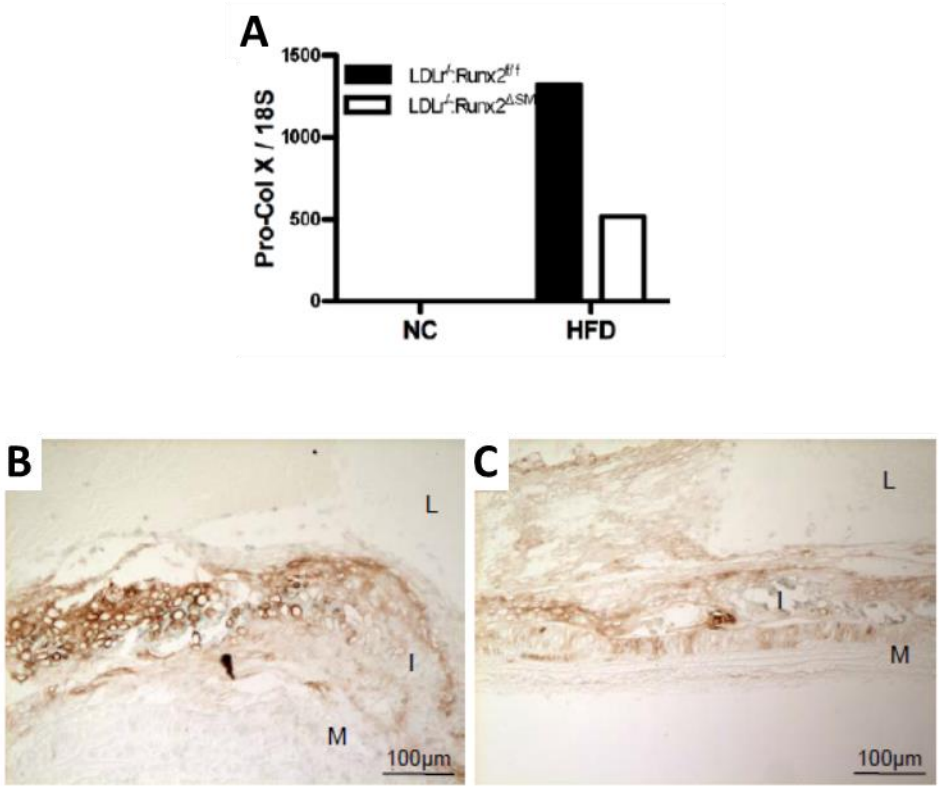

Figure 3.8: Col X expression decreased in Runx2$^{\Delta SM}$ mice.

LDLr$^{-/-}$:Runx2$^{f/f}$ and LDLr$^{-/-}$:Runx2$^{\Delta SM}$ mice were fed with normal chow (NC) or high fat diet (HFD) for 18 **(A)** and 24 weeks **(B** and **C)**. 18-week aortic arches were pooled for RNA extraction and quantitative RT-PCR of Col X (n = 5 – 7). Data shown are one of the two RNA preparations. 24-week aortic arches were collected from HFD animals for immunohistochemical staining (brown) of Col X **(B** and **C).**

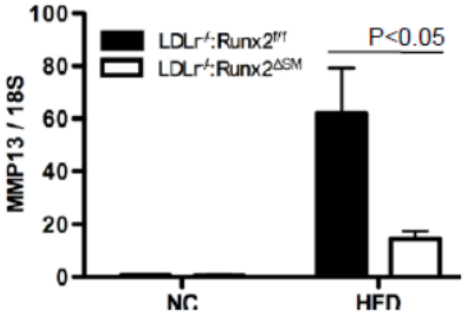

Figure 3.9: MMP13 RNA expression decreased in Runx2$^{\Delta SM}$ mice.

LDLr$^{-/-}$:Runx2$^{f/f}$ and LDLr$^{-/-}$:Runx2$^{\Delta SM}$ mice were fed with normal chow (NC) or high fat diet (HFD) for 18 week. Aortic arches were pooled from triplicate RNA extractions and quantitative RT-PCR of MMP13 was performed (n = 5 – 7). Data shown are Mean ± S.E.M.

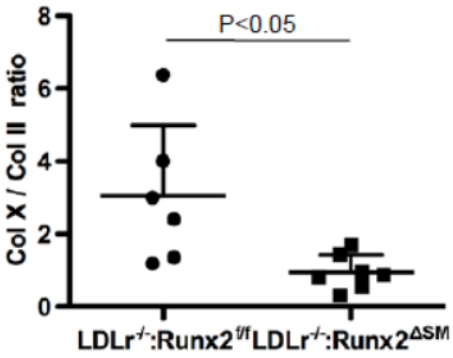

Figure 3.10: Col X to Col II ratio decreased in Runx2$^{\Delta SM}$ mice.

LDLr$^{-/-}$:Runx2$^{f/f}$ and LDLr$^{-/-}$:Runx2$^{\Delta SM}$ mice were fed with normal chow (NC) or high fat diet (HFD) for 24 weeks. Aortic arches were collected from HFD animals. Quantitation of Col II and Col X immunohistochemical staining was used to determine relative expression.

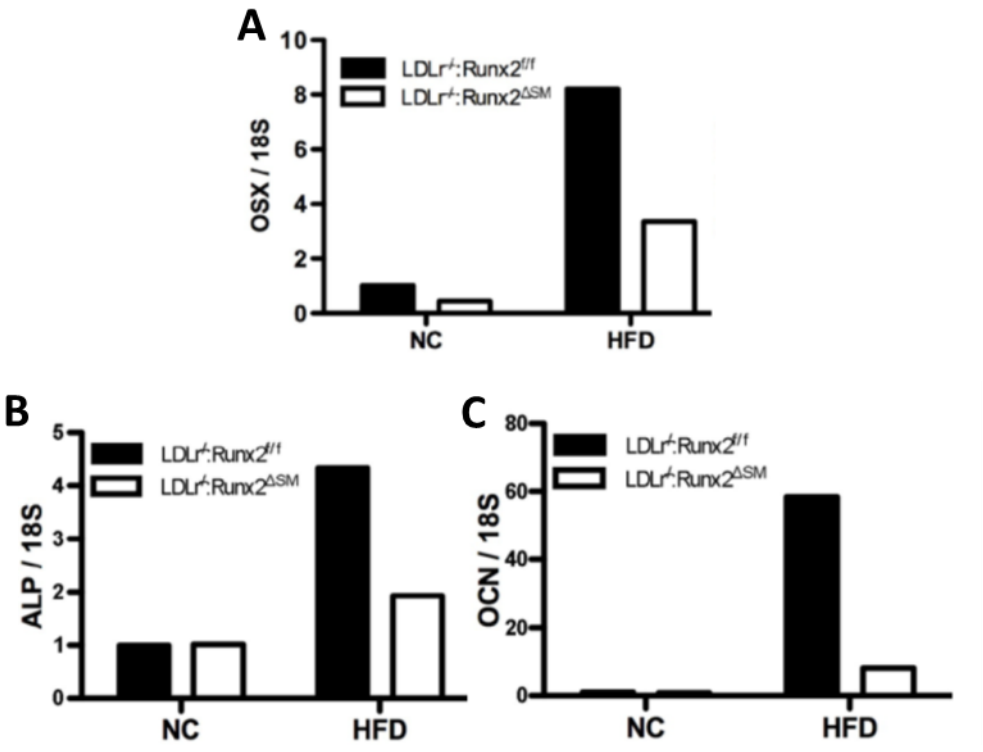

Figure 3.11: SMC-specific Runx2 removal prevents osteogenic differentiation.

$LDLr^{-/-}$:$Runx2^{f/f}$ and $LDLr^{-/-}$:$Runx2^{\Delta SM}$ mice were fed with normal chow (NC) or high fat diet (HFD) for 18 weeks. Aortic arch RNA was used to determine osteogenic differentiation of SMCs via quantitative RT-PCR for osterix (OSX), alkaline phosphatase (ALP) and osteocalcin (OCN) (**A - C**). Data shown are one of the two RNA preparations. Similar results were achieved in another independent RNA extraction.

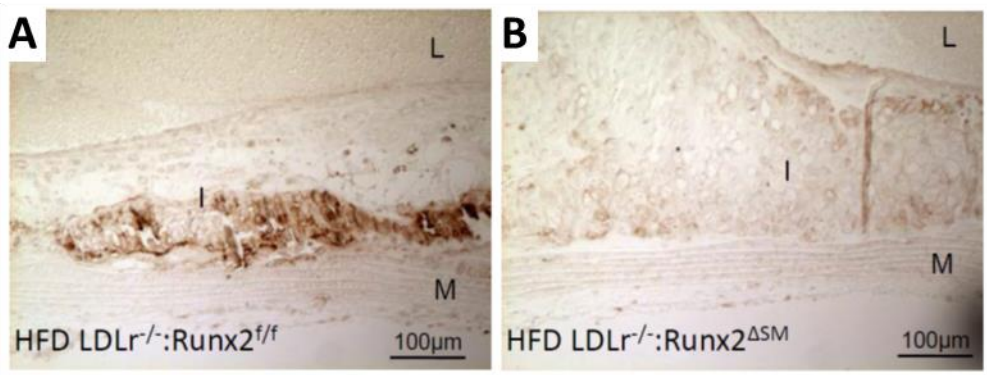

Figure 3.12: OCN expression was reduced atherosclerotic vasculature of Runx2$^{\Delta SM}$ mice. LDLr$^{-/-}$:Runx2$^{f/f}$ and LDLr$^{-/-}$:Runx2$^{\Delta SM}$ mice were fed with normal chow (NC) or high fat diet (HFD) for 24 weeks. Aortic arches were collected from HFD animals for immunohistochemical staining (brown) of OCN.

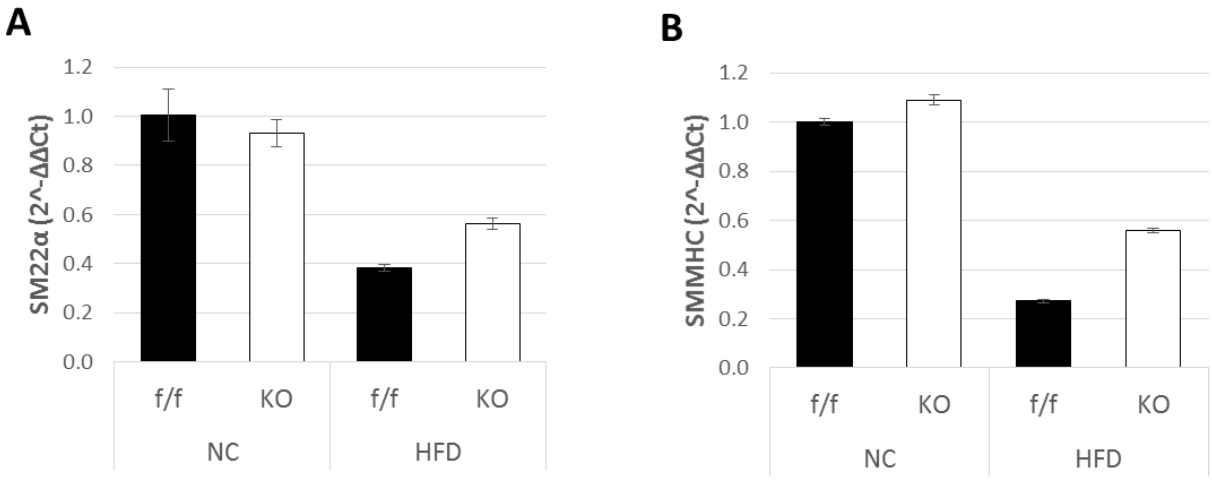

Figure 3.13: SMC-specific Runx2 removal partially rescues smooth muscle marker expression.

LDLr$^{-/-}$:Runx2$^{f/f}$ and LDLr$^{-/-}$:Runx2$^{\Delta SM}$ mice were fed with normal chow (NC) or high fat diet (HFD) for 18 weeks. Aortic arch RNA was used to determine smooth muscle marker expression of SMCs via quantitative RT-PCR for SM22α and SMMHC (**A** and **B**).

4 Chapter 4: Determining the role of Runx2 in macrophage content and polarization in AIC

4.1 Abstract

Macrophages represent a significant but diverse cell population in atherosclerotic lesions. They exhibit phenotypic and functional heterogeneity and can switch or "polarize" from one polarity to another. Macrophage polarization in the context of atherosclerotic lesion progression and regression remains poorly defined. In this chapter, we show that smooth muscle-specific Runx2 expression does not affect atherosclerotic lesion size or macrophage infiltration and polarization, despite a reduction in calcification. These findings demonstrate a cell autonomous and pathway specific nature of Runx2 in arterial intimal calcification and are the first to present a genetic separation of the calcific sclerotic process from the lipid laden, atherogenic process. We propose to further investigate the effect of Runx2 on polarization of lesional macrophages. In atherosclerotic aortas, deletion of Runx2 in SMCs resulted in a shift in macrophage polarization toward an alternatively activated or M2 polarization. We used a co-culture model of SMCs and RAW264.7 cells to test the hypothesis that Runx2 mediates smooth muscle signaling of macrophages. In support of this hypothesis, we found significant increases in expression of two M2 markers: MRC1 and IR-1R2. We determined the mechanism through which Runx2 mediates IL-1R2 expression was through an IL-4 independent pathway. To our knowledge, these results are the first to show that SMCs can directly alter macrophage polarization, and has promising implications for treatments looking to regulate macrophage polarization in atherosclerotic lesions.

4.2 Introduction

4.2.1 Atherosclerosis

Arterial intimal calcification (AIC) is the most common form of calcific vasculopathy and is heavily associated with atherosclerosis.[8] Atherosclerotic plaques result from a failure to resolve the inflammatory response initiated by the accumulation and retention of cholesterol-rich, apolipoprotein B-containing lipoproteins, mainly low-density lipoproteins (LDL) in the arterial wall. These sequestered LDLs are subject to various modifications, enabling endothelium activation and inflammatory response of circulating mononuclear cells, resulting in accrual and activation of macrophages and T lymphocytes in the subendothelial space of blood vessels. Although plaques can have substantial variations in thickness of fibrous caps, atheroma size, cell type, and extent of calcification, only specific types of lesions are associated with acute manifestations of atherosclerotic disease.[85] Mortality from atherosclerosis stems from the rupture of unstable plaques, leading to thrombosis and subsequent myocardial infarction and stroke. Since there are no medications targeting lesion regression, it is of particular interest to explicate mechanisms governing plaque stability for development of potential therapeutics.

4.2.2 Macrophage polarization and vascular calcification

Macrophages play a key role in initiation, progression, and regression of atherosclerotic plaques.[86–88] They exhibit phenotypic and functional heterogeneity, as evidenced by a wide spectrum of activational programs that exist as a function of their immediate surroundings, including lipids and their derivations, various cytokines, calcium/phosphate minerals, and microbial moieties.[86] Due to this heterogeneity, macrophages can either promote or prevent disease progression depending on the phenotype it assumes.

This dual role of macrophages has commonly been characterized by dividing them into pro-inflammatory (M1) and pro-healing (M2) classifications. M1 macrophages, induced by T-helper 1 (Th1) cytokines such as interferon-γ (IFN-γ), have been found in rupture-prone shoulder regions of human atherosclerotic plaques.[89] They are believed to maintain local inflammation and contribute to degradation of the extracellular matrix, thereby leading to plaque destabilization and increased risk of rupture.[25,89] TNFα and IL-6, two cytokines associated with M1 macrophages, have also been implicated in macrophage-mediated SMC calcification.[90,91] On the other hand, pro-healing (M2) macrophages, induced by Th2 cytokines such as key M2 mediator interleukin-4 (IL-4), have been implicated in wound healing, plaque stability, and regression of plaques. M2 macrophages are located far from the lipid core, predominantly in stable, cell-rich areas of the plaque and adventitia.[89,92] Increased numbers of M2 macrophages have been observed in models of atherosclerotic regression and appear to play a major role in inflammation resolution and plaque remodeling.[93]

In recent years, the classical M1/M2 distinction has been further expounded due to the recognition of greater heterogeneity of macrophage phenotypes. Interestingly, further analyses of macrophages in mice atherosclerotic lesions have shown that M1 and M2 macrophages only comprise 40% and 20%, respectively, of total lesional macrophages.[94] A distinct macrophage phenotype (termed Mox) has been observed to comprise 30% of all macrophages in advanced mouse atherosclerotic lesions, although this phenotype has yet to be confirmed in human specimens.[88,94] Because limited studies have examined the link between macrophage polarization with atherosclerotic lesion progression and regression, it is unclear how macrophage phenotypes

are regulated during atherosclerotic lesion progression and regression, and whether macrophage polarization is critical for plaque vulnerability or a consequence of it.[95]

Drug therapies for treatment of VC and atherosclerosis are still lacking. Current pharmacological therapies for atherosclerosis are still focused on cholesterol control (statins and CETP inhibitors), glucose control, and anti-platelet approaches that target lesion progression.[96] There are no medications targeting lesion regression. It has been suggested that inducing macrophages toward an anti-inflammatory, wound-healing M2 polarization might be important in regressing and stabilizing atherosclerotic plaques by secreting anti-inflammatory factors, promote tissue remodeling and repair, and clearance of necrotic debris.[86] Inflammation also frequently accompanies atherosclerotic vascular calcification. Macrophages in atherosclerotic lesions produce proinflammatory cytokines, which may induce SMC apoptosis and osteochondrogenic differentiation leading to calcification.[90] Experimental evidence suggests a causal link between inflammatory cytokines and development of calcification, and further study in this area could reveal clinical approaches for prevention and treatment.[91,97] Thus, in this chapter, we aim to determine the role of Runx2 in macrophage polarization in atherosclerotic plaques with the goal of identifying potential targets for prevention and treatment of VC.

4.3 **Materials and Methods**

4.3.1 Mouse model for vascular intimal calcification

The same mouse model was used as outlined in **Chapter 3.3.1:** Mouse model for vascular intimal calcification (page 34).

4.3.2 Morphometric analysis of atherosclerosis and macrophage content

Sample collection for atherosclerotic lesion and macrophage content analyses were outlined in **Chapter 3.3.2:** Morphometric and immunohistochemical analysis of atherosclerotic vessels and cartilaginous metaplasia (page 35). Movat pentachrome staining was used to visualize atherosclerotic lesions. Intimal lesion areas were measured blindly and normalized to the length of internal elastic lamina (for longitudinal sections of aortic arches) or area of arterial media (for cross sections of brachiocephalic arteries) using Metamorph software (Molecular Device). MOMA2 (MCA519G, AbD Serotec) antibody was used to detect macrophages immunohistochemically. Macrophages were identified by MOMA2 antibody, quantified with the same sampling scheme, and expressed as percent intimal area.

4.3.3 *In vitro* calcification assay

Runx2$^{\Delta SM}$ and Runx2$^{f/f}$ SMCs were seeded at 2.0 x 10^4 cells/well into 6-well plates. At ~70-80% confluency, treatment began with culture media supplemented with 2.4 mM inorganic phosphate and continued for 4 or 9 days. Media was changed every other day.

4.3.4 Quantitative RT-PCR

Total RNA was extracted from aortic arches (**4.3.1**) or SMC monolayers (**4.3.3**) and used to synthesize first-strand cDNA using Omniscript (Qiagen) at 37°C for 1 hour. The cDNA produced was used to determine expression of M1 macrophage markers: tumor necrosis factor (TNF), interleukin 12B (IL-12B), interferon gamma (IFN-γ), interleukin 6 (IL-6), and interleukin 1 beta (IL-1β), and M2 macrophage markers: chitinase-like 3 (Ym1), interleukin 10 (IL-10), interleukin 4 (IL-4), arginase I (Arg1), mannose receptor, C type 1 (MRC1), and interleukin 1 receptor 2 (IL-1R2) using Taqman quantitative RT-PCR. Primers/probes of *Tnf* (Mm00443258_m1), *Il12b* (Mm00434174_m1), *Ifnγ* (Mm01168134_m1), *Il6*

(Mm00446190_m1), *Il1b* (Mm00434228_m1), *Ym1* (Mm00657889_mH), *Il10* (Mm00439614_m1), *Il4* (Mm00445259_m1), *Arg1* (Mm00475988_m1), *MRC1* (Mm00485148_m1), and *Il1r2* (Mm00439629_m1) were purchased from Life Technologies.

All the probe sequences span an exon-exon junction of the desired genes to avoid amplification of residual genomic DNA. 18s ribosomal RNA expression was determined using Taqman Ribosomal RNA Control Reagents (ABI) to control sample loading. Gene expression levels were determined in triplicates, normalized to 18s ribosomal RNA levels and expressed as a fold of control samples. For *in vivo* studies, RNA expression was normalized to expression of vessels from $Runx2^{f/f}$ mice fed with NC diet for 18 weeks. For *in vitro* experiments, RNA expression was normalized to expression of $Runx2^{f/f}$ SMCs in cultured in normal media for 4 or 9 days.

4.3.5 IL-4 ELISA assay

$Runx2^{\Delta SM}$ and $Runx2^{f/f}$ SMCs were seeded at 2.5 x 10^4 cells/well in triplicate in 6-well plates, supplemented with 10% FBS. Prior to collection, culture media (DMEM supplemented with 10% FBS and 1% antibiotics) was changed to either 0 % or 0.5% FBS at 800 µL/well media. Supernatant was collected at 3 or 24 hours, and centrifuged at 14,000 rpm for 10 min at 4 ºC to remove cells and cellular debris.

A Mouse IL-4 DuoSet ELISA (DY404-05, R&D) was used to quantify IL-4 secretion. Briefly, 96-well microplates were coated with capture antibody (4.0 µg/mL) and incubated overnight. Wells were washed with buffer several times prior to addition of blocking solution, and washed again. For sample detection, 100 µL standards or SMC conditioned media were added directly to each well, washed, and detection antibody (600 ng/mL) was added. Following another wash,

Streptavidin-HRP solution was added and the plate was incubated with minimal light. After another wash step, a substrate solution (H_2O_2 and tetramethylbenzidine) was added, followed by a stop solution (2N H_2SO_4). The plate was immediately read at 450 nm with wavelength correction at 540 nm. The standard curve was made using serial dilutions of IL-4 ranging from 7.82 pg/mL to 500 pg/mL.

4.3.6 Co-culture study

Runx2$^{\Delta SM}$ and Runx2$^{f/f}$ SMCs were seeded at 3 x 10^4 cells/well into Transwell inserts in triplicate. After 2 days, RAW264.7 cells were seeded at 5 x 10^4 cells/well in 6-well plates in triplicate. The following day, SMCs and RAW264.7 cells were brought together to begin co-culture studies (**Figure 4.1**). RNA was collected from RAW264.7 cells after 6 and 24 hours of co-culture using an RNeasy Mini Kit (Qiagen) and prepared for quantitative RT-PCR. Treatment of RAW264.7 cells in serum free media with 50 ng/mL recombinant IL-4 (eBioscience, 14-8041-62) for 6 hours was used as a positive control for macrophage induction.

4.3.7 Statistics

Data shown as means ± S.D., were analyzed with Student's t-test. Data were considered to be statistically significant at a p value < 0.05.

4.4 **Results**

4.4.1 Runx2 deletion does not block atherosclerotic lesion formation

To determine whether deletion of Runx2 in SMCs affected lesion formation, histomorphometric analyses were performed on aortic arches and brachiocephalic arteries of Runx2$^{f/f}$ and Runx2$^{\Delta SM}$ mice fed a HFD. As shown in **Figure 4.2**, arteries from Runx2$^{f/f}$ and Runx2$^{\Delta SM}$ mice had typical atherosclerotic lesions, containing foam cells, cartilaginous metaplasia, necrotic core, and fibrous

caps. Quantitation of lesion size at either arterial site showed no significant difference between genotypes (**Figure 4.3A** and **B**), indicating that Runx2 in SMCs is not required for atherosclerotic lesion formation and development in HFD-fed LDLr$^{-/-}$ mice.

4.4.2 Runx2 deletion does not inhibit RANKL expression or macrophage content of lesions

Macrophage infiltration and foam cell formation are major processes required for atherosclerotic lesion formation in mouse models, including ApoE$^{-/-}$ and LDLr$^{-/-}$ mice.[54,98] We observed abundant monocyte/macrophage accumulation in aortic arches and brachiocephalic arteries of HFD fed Runx2$^{f/f}$ mice (**Figure 4.4A** and **D**), and comparable levels in Runx2$^{\Delta SM}$ mice that lack functional, truncated Runx2 protein (**Figure 4.4B** and **E**). Quantification of MOMA2 expression showed no differences due to genotype, location, or length of diet (**Figure 4.5**). Furthermore, mRNA expression of RANKL, MCP1 (a macrophage recruitment ligand) and CCR2 (its receptor) was not altered in Runx2$^{f/f}$ aortas compared to Runx2$^{\Delta SM}$ aortas (**Figure 4.6**).

4.4.3 Runx2 removal increases M2 marker expression in atherosclerotic lesions

Mice fed with a high fat diet (HFD) for 18 weeks showed increased expression of M1 (TNF, IL-12B, IFNγ, IL-6, and IL-1β) and M2 (Ym1, IL-10) markers compared to mice fed with normal chow (NC), suggesting a shift in macrophage content and polarization in the lesions of HFD fed mice (**Figure 4.7** and **Figure 4.8**). Removal of Runx2 resulted in marked increases in several M2 markers in HFD fed mice, including an 885% increase in Arg1 expression, a 136% increase in MRC-1 expression, a 110% increase in Ym1 expression, and a 42% increase IL-10 expression (**Figure 4.7**). While most M1 markers remained relatively unchanged (TNF, IL-12B, IFNγ), expression of IL-1β (a pro-inflammatory cytokine) was increased over four-fold in Runx2$^{\Delta SM}$

HFD samples (**Figure 4.8D**). Changes in marker expression were scored and summarized (**Table 4.1**).

4.4.4 Runx2 removal increases IL-4 mRNA expression in SMCs

IL-4 is often found in atherosclerotic lesions associated with M2 macrophages and is a known potent Th2 cytokine that directs M2 macrophage polarization in culture.[88,92,99] We observed no difference in IL-4 mRNA expression between control and Runx2$^{\Delta SM}$ whole aorta samples (data not shown). We then analyzed IL-4 expression in isolated Runx2 knockout (Runx2$^{\Delta SM}$) SMCs in comparison to the Runx2$^{f/f}$ control cells (**Figure 4.9**). In the absence of Runx2, SMCs showed a 3-fold increase in IL-4 mRNA expression, whereas another Th2 cytokine, IL-13, and Th1 cytokines, IL-1β and TNFα, were barely detectable. We tested the hypothesis that induction was independent of SMC calcification, and found that these results were independent of the addition of procalcific media.

4.4.5 IL-4 secretion was undetectable in SMCs in culture

We observed differences of IL-4 RNA expression and then tested whether IL-4 protein secretion differed between cultured Runx2$^{\Delta SM}$ and Runx2$^{f/f}$ SMCs. SMCs were cultured for 3 or 24 hours in 0% or 0.5% FBS. Using an ELISA for IL-4, we measured IL-4 levels in culture media and determined that secreted IL-4 from SMCs was undetectable in culture (less than 7.8 pg/mL). This data suggests that IL-4 is not critical for Runx2-mediated SMC signaling.

4.4.6 Co-culture of SMCs and RAW264.7 cells

We hypothesized that Runx2 removal in VSMCs could increase M2 polarization of RAW264.7 cells, and tested this hypothesis by co-culturing Runx2$^{\Delta SM}$ or Runx2$^{f/f}$ SMCs with RAW264.7 for 6 or 24 hours. RNA was extracted from RAW264.7 cells and analyzed via quantitative RT-PCR

for M2 macrophage markers. We focused our analyses on M2 markers that we had previously identified as biomarkers that exhibit increased expression in mouse atherosclerotic aortas. MRC1 expression was increased 148% at 6 hours ($p < 0.03$), while pronounced but not significant induction was observed for IL-10 (**Figure 4.10A** and **B**). No significant differences were observed among other markers (Arg1, IL-4) (**Figure 4.10C** and **D**).

IL-1R2 is a known M2 marker which acts a decoy receptor for IL-1R1 due to its lack of an intracellular signaling domain (**Figure 4.10E**). RAW264.7 cells incubated with $Runx2^{\Delta SM}$ SMCs exhibited a six-fold increase in IL-1R2 RNA expression over $Runx2^{f/f}$ SMCs at 6 hours of co-culture ($p < 0.03$). This effect was attenuated by 24 hours. Treatment of RAW264.7 cells with recombinant IL-4 was used for positive controls. Arg1, MRC1, and IL-10 showed significant induction following treatment, while IL-4 and IL-1R2 expression were not induced by recombinant IL-4 (**Figure 4.11**).

4.5 Discussion

In this chapter, we found that removal of Runx2 in vascular SMCs did not affect atherosclerotic lesion size, monocyte/macrophage recruitment, and RANKL expression. Taken together with our findings from **Chapter 3**, these findings demonstrate a cell autonomous and pathway specific nature of Runx2 in AIC and are the first to present a genetic separation of the calcific sclerotic process from the lipid laden, atherogenic process. These findings suggest that different mechanisms regulate the formation and progression of calcification and atheroma, two major pathological features often observed in advanced atherosclerotic lesions.

It's important to note that our findings regarding monocyte/macrophage infiltration and lesion size noticeably differed from a recent study by Sun *et al*.[49] In that study, the authors found significantly reduced SMC elaboration of RANKL, a TNF family member important for monocyte infiltration and differentiation of mineral-resorbing osteoclasts, along with a near complete inhibition of monocyte/macrophage recruitment and atherosclerosis.[49,100,101] Notably, AIC was completely eliminated, likely due to the inhibition of oxidative stress-dependent osteogenic differentiation and osteoblast-osteoclast crosstalk. In their model, the authors showed production of a truncated Runx2 protein following genomic recombination.[49] Their findings can be explained by the truncated Runx2 protein acting via a dominant negative effect on the Runt-related family members in addition to Runx2, specifically Runx1 and Runx3 which share the same vital runt DNA binding domain and are involved in regulating monocyte/macrophage biology.[50,67–70] The authors showed that the truncated protein was detectable via an EMSA supershift assay and maintained ~30% functional activity via a Runx2 luciferase reporter.[49] Our approach of targeting exon 4, which codes the Runt homology domain, directly addresses limitations of that model and minimizes the risk and scope of off-target effects should a truncated Runx2 protein still be produced.

We demonstrated that Runx2 does not alter monocyte/macrophage infiltration in atherosclerotic vessels at both the translational and protein levels, despite a reduction of calcification in the lesion. Thus, we hypothesized that altered polarization of macrophages could help explain our enigmatic findings. Macrophage polarization plays an immensely important role in their function and regulation of plaque stability, potentially through regulation of matrix vesicle shedding, which may initiate microcalcification.[54]

In Runx2$^{\Delta SM}$ and Runx2$^{f/f}$ mice fed with a high fat diet, removal of Runx2 resulted in increased expression of M2-associated markers, including Arg1, MRC1, Ym1, and IL-10 (**Figure 4.7**). These findings indicate a shift in macrophage polarization toward an alternatively activated or M2 polarization. No consistent, overall differences in expression were observed between most M1 markers upon Runx2 loss. Notably, expression of IL-1β (a pro-inflammatory cytokine) was increased over four-fold in Runx2$^{\Delta SM}$ samples (**Figure 4.8**). Surprisingly, IL-1β has been implicated in induction of M2b macrophages, a subtype of M2 macrophages.[95,102] Although commonly associated with an inflammatory phenotype, IL-1 signaling also has been shown to promote plaque stabilization, increase lesional collagen content, reduce intraplaque hemorrhage, and boost SMC numbers in atherosclerotic plaques, properties usually associated with an M2 (pro-healing) polarization.[103] Our findings indicate that Runx2 plays a key role in preventing SMCs from inducing macrophages toward an M2 polarization, and that its removal may allow macrophages to further stabilize atherosclerotic plaques despite a concurrent reduction in overall calcification.

In our *in vitro* studies, we detected a three-fold procalcific media-independent induction of IL-4 expression in SMCs lacking Runx2 (**Figure 4.9**). Other M1 (IL-1β and TNFα) and M2 (IL-13) markers were barely detectable, despite high expression in mouse atherosclerotic aortas. Our data suggested that IL-4 may play a role in paracrine signaling in Runx2 mediated macrophage polarization. We next sought to measure IL-4 secretion to determine if protein levels mirrored our RNA expression data. Using an ELISA for IL-4, we were unable to detect IL-4 secretion in

culture media (<7.82 pg/mL) and were thus unable to detect any differences in the absence of Runx2.

While we had initially hypothesized otherwise, it is also not surprising that we were unable to detect IL-4 secretion from vascular SMCs, despite detecting significant amounts at the mRNA level. All mRNAs are not equal with regard to translation into proteins. There are a multitude of post-translational mechanisms which control protein half-lives and trafficking within the cell. Considering the process through which IL-4 may need to be secreted and what we already know about its short half-life *in vivo*, it is unsurprising that detection of secreted IL-4 may not be feasible.[104,105] Additionally, no studies have looked at or detected IL-4 expression in smooth muscle cells at either the RNA or protein level. The search for IL-4-producing cells (besides T cells) is critical for understanding the induction of naïve T cells. These cell sources are still subject to considerable debate,[106] and identifying one is a nontrivial goal. Although we hypothesized a smooth muscle source for IL-4, our data suggests an alternative mechanism for SMC-macrophage signaling.

To further study the effect of Runx2-mediated smooth muscle signaling of macrophages, we used a co-culture model of vascular SMCs and RAW264.7 cells. In SMCs without Runx2, common M2 markers MRC1 and IL-1R2 exhibited significant increases of 148% and 501%, respectively, in mRNA expression at 6 hours while other markers examined did not show statistically relevant changes (**Figure 4.10A** and **E**). By 24 hours, however, neither of the two genes were significantly different. IL-1R2, in particular, has been shown to be quickly

upregulated and has a short half-life in murine cells, indicating its role as an early response gene.[107] These data suggest SMC signaling of macrophages may be quick but short-lived.

Although further studies are needed, upregulation of both a ligand (IL-1β in mouse atherosclerotic aortas) and its decoy receptor (IL-1R2 in RAW264.7 cells) offers an interesting dynamic and paints a more nuanced picture of Runx2-mediated macrophage signaling by SMCs. While the exact role of IL-1R2 remains unclear, current literature reinforces its growing importance in the development of atherosclerosis. Clinically, macrophages in hyperlipidemic patients have decreased IL-1R2 mRNA and protein expression, which may facilitate IL-1 signaling.[108] Studies have shown that in $ApoE^{-/-}$ mice (another model for atherosclerosis), treatment with IL-1 receptor antagonist (IL-1RA, another negative regulator of IL-1) decreased lesion sizes.[109] In our studies, we found that treatment of only RAW264.7 cells with recombinant IL-4 did not result in induction of IL-1R2, despite significant induction of other M2 markers (notably Arg1, MRC1, and IL-10) (**Figure 4.11**). This suggests that the mechanism through which Runx2 mediates IL-1R2 expression in RAW264.7 cells is through an IL-4 independent pathway. IL-4 is the canonical inducer for M2 macrophages. However, macrophages can also be induced toward M2 polarization through a diverse range of environmental signals.[110]

4.6 Conclusions

In this chapter, we showed that atherosclerotic lesion size and monocyte/macrophage infiltration are not affected by SM-specific expression of Runx2. Our results suggest that different mechanisms regulate the formation and progression of calcification and atheroma. They support that lack of Runx2 in SMCs enhanced its ability to induce macrophages toward an M2 polarization in a co-culture system. These results further reinforce our *in vivo* findings and

suggest a direct induction between the two cell types. While accompanying factors remain to be identified, paracrine and contact-independent signaling appear to be essential for smooth muscle-induced M2 polarization of macrophages. To our knowledge, these results are the first to demonstrate that SMCs can directly alter macrophage polarization, and has promising implications for treatments looking to regulate macrophage phenotype in atherosclerotic lesions.

4.7 Figures

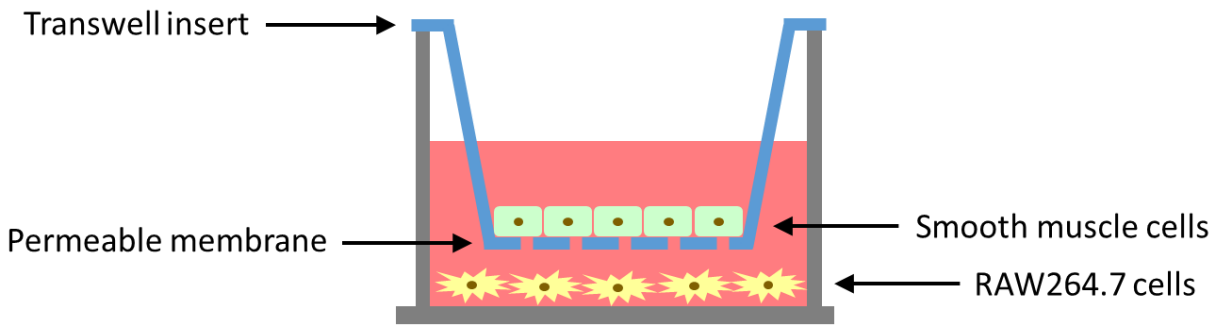

Figure 4.1: Experimental design for co-culture of SMCs and RAW264.7 cells.

Isolated Runx2$^{f/f}$ or Runx2$^{\Delta SM}$ SMCs were seeded in the Transwell insert, while RAW264.7 cells were seeded directly into 6-well plates.

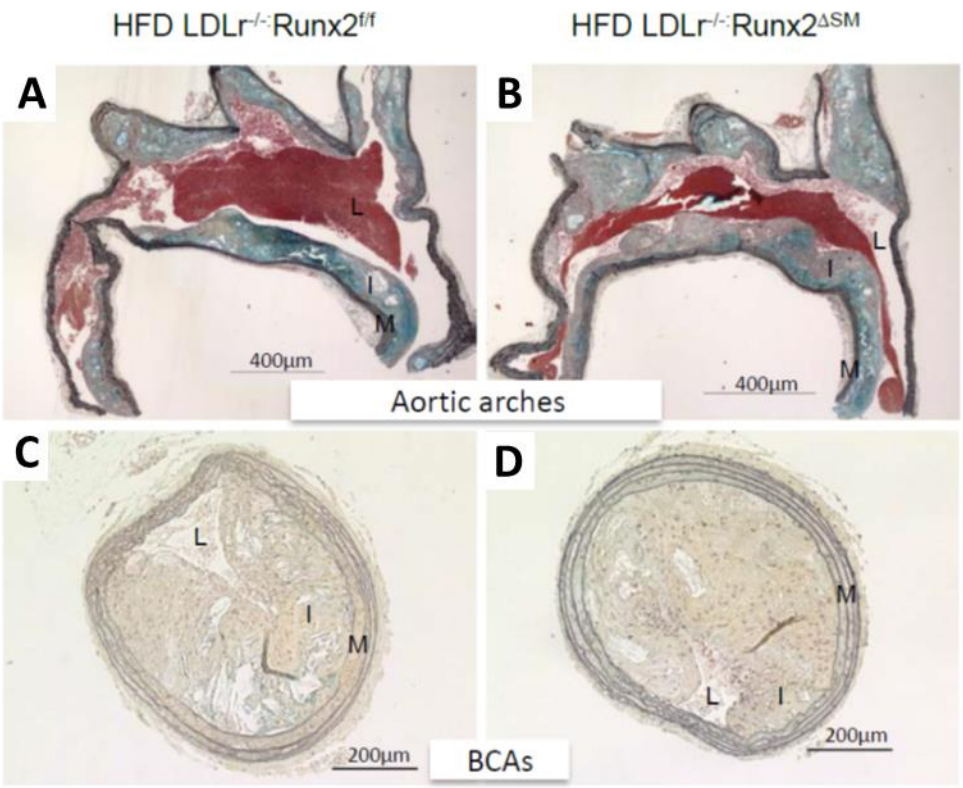

Figure 4.2: SMC-specific Runx2 removal does not alter atherosclerotic lesion progression. Sections were taken from aortic arches (**A** and **B**) and brachiocephalic arteries (BCA; **C** and **D**) of 24 weeks HFD-fed LDLr$^{-/-}$:Runx2$^{f/f}$ and LDLr$^{-/-}$:Runx2$^{\Delta SM}$ mice and processed with Movat pentachrome staining.

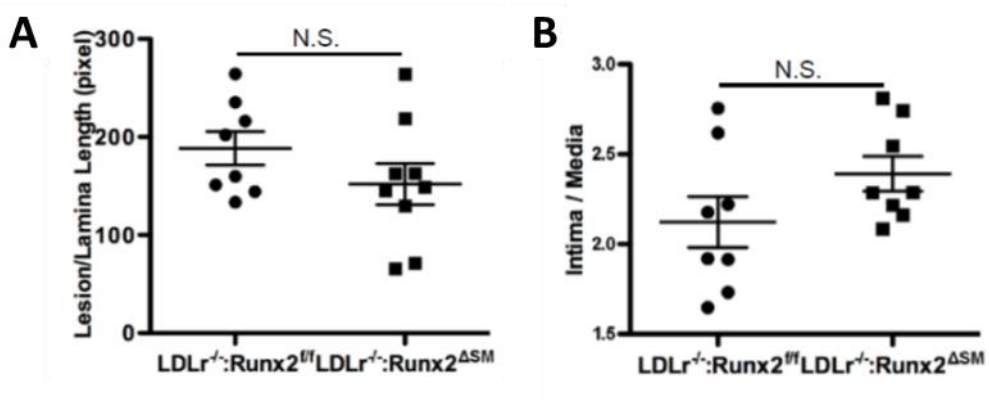

Figure 4.3: Quantification of atherosclerotic lesion progression.

Serial sections from aortic arches **(A)** and brachiocephalic arteries **(B)** of 24 weeks HFD-fed LDLr$^{-/-}$:Runx2$^{f/f}$ and LDLr$^{-/-}$:Runx2$^{\Delta SM}$ mice were used to evaluate atherosclerotic lesion progression. Intima area was measured morphometrically as described in Materials and Methods. Data shown are Mean ± S.E.M (n = 8–9).

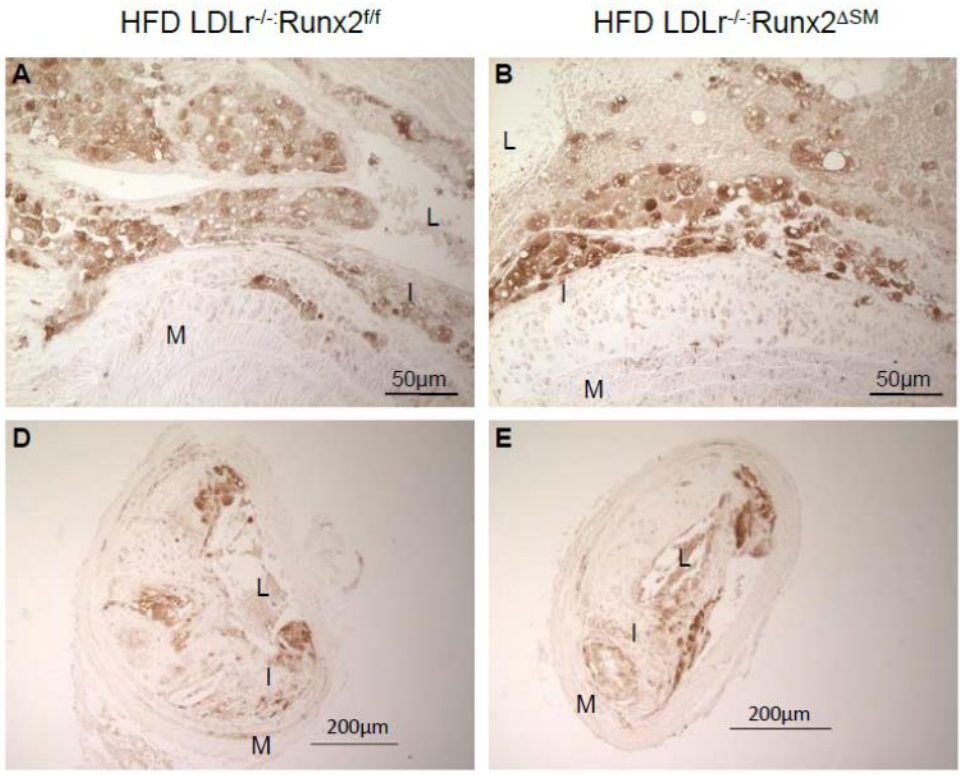

Figure 4.4: SMC-specific Runx2 removal does not alter monocyte/macrophage infiltration. Monocyte/macrophage infiltration was visualized using MOMA2 antibody in 18-week aortic arches (**A, B**) and BCA (**D, E**) of HFD LDLr$^{-/-}$:Runx2$^{f/f}$ (A and D) and LDLr$^{-/-}$:Runx2$^{\Delta SM}$ (B and E) mice.

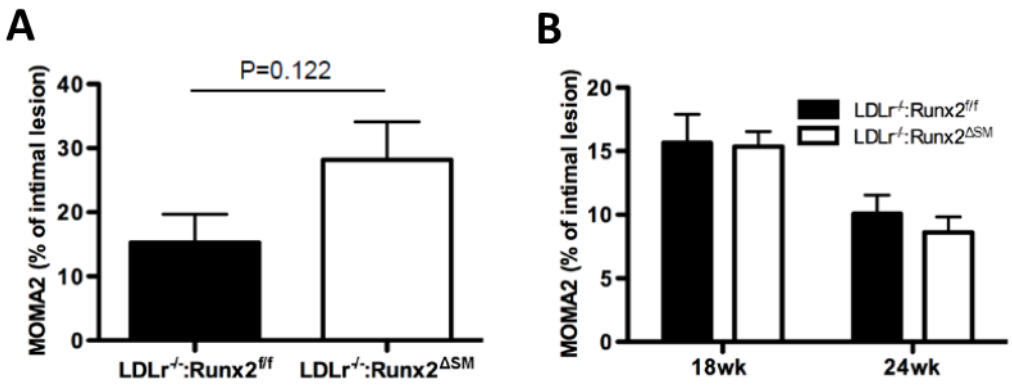

Figure 4.5: Quantification of MOMA2 expression in Runx2$^{\Delta SM}$ aortas.

Monocyte/macrophage infiltration was quantified using MOMA2 antibody in 18-week aortic arches and BCA of HFD Runx2$^{f/f}$ and Runx2$^{\Delta SM}$ mice. Quantification of MOMA2 positive area for both 18 week aortic arches as well as 18 and 24 week BCA were shown in **A** and **B** respectively (n = 4 – 8). Data shown are Mean ± S.E.M.

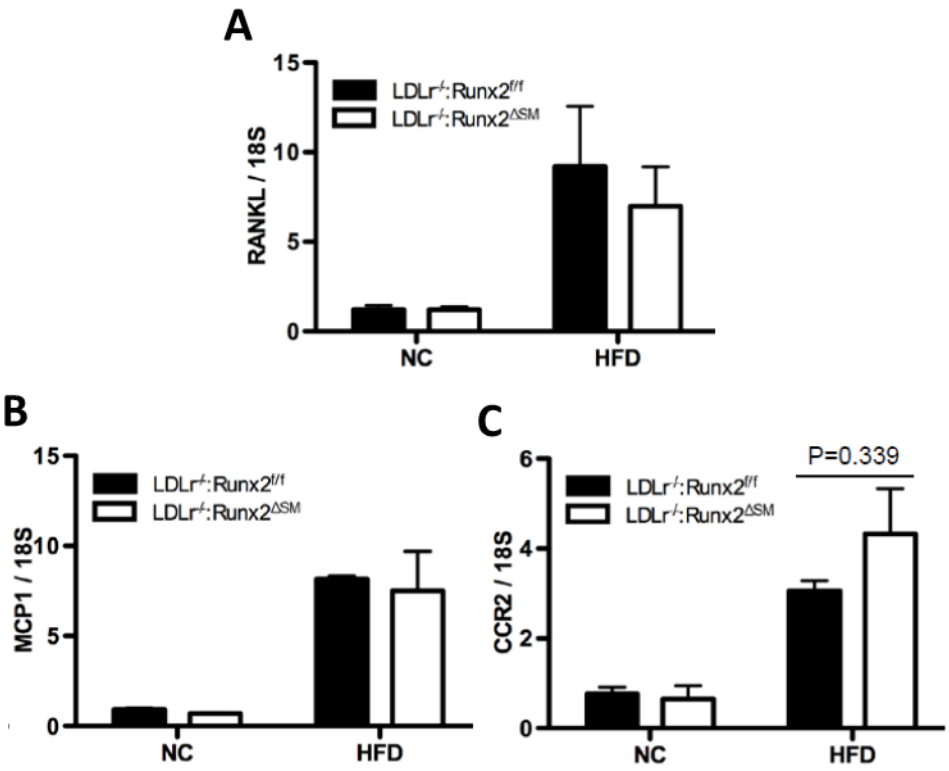

Figure 4.6: SMC-specific Runx2 removal does not alter macrophage markers and RANKL expression.

Expression of RANKL, a critical chemoattractant during monocyte/macrophage infiltration, MCP1, and its receptor CCR2, are evaluated using triplicate RNA samples extracted from pooled 18-week aortic arches (**A-C**, n = 9 – 12). Data shown are Mean ± S.E.M.

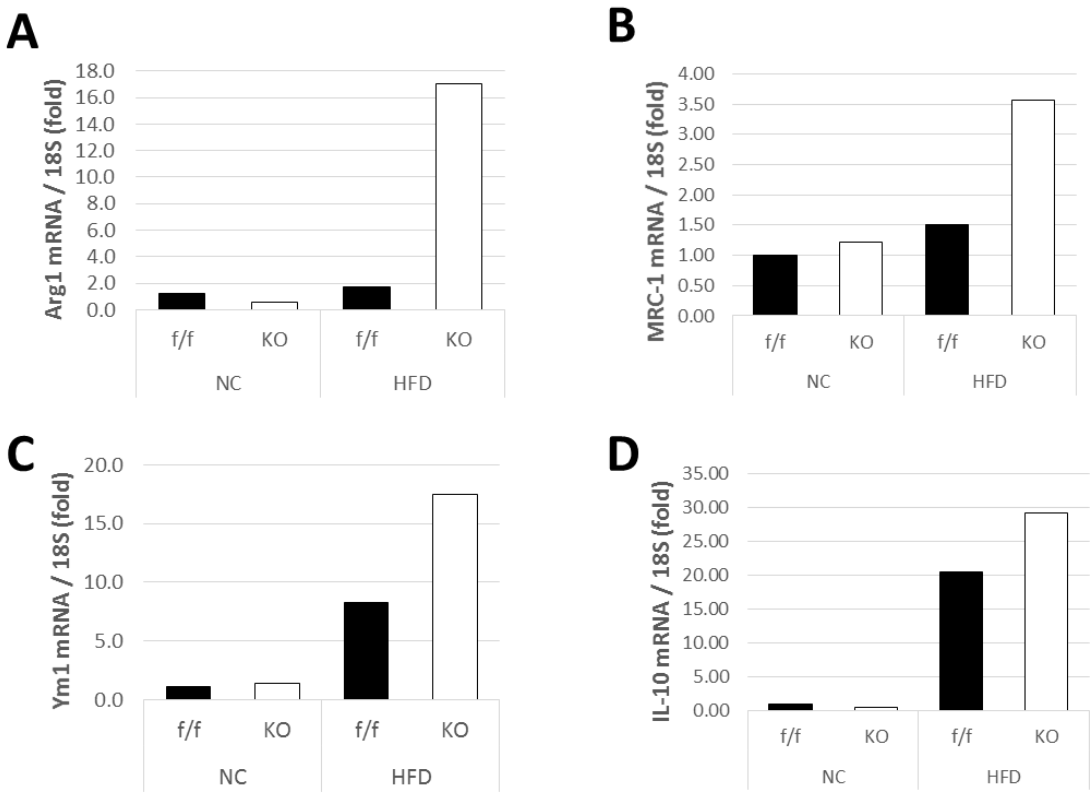

Figure 4.7: Removal of Runx2 increases M2 marker expression in atherosclerotic lesions. Gene expression of M1 and M2 markers was determined by quantitative RT-PCR using pooled aortic arches. Expression of *Arg1* **(A)**, *MRC-1* **(B)**, *Ym1* **(C)**, and *IL-10* **(D)** using quantitative RT-PCR using pooled aortic arches from pooled 18 week HFD mice (n = 3).

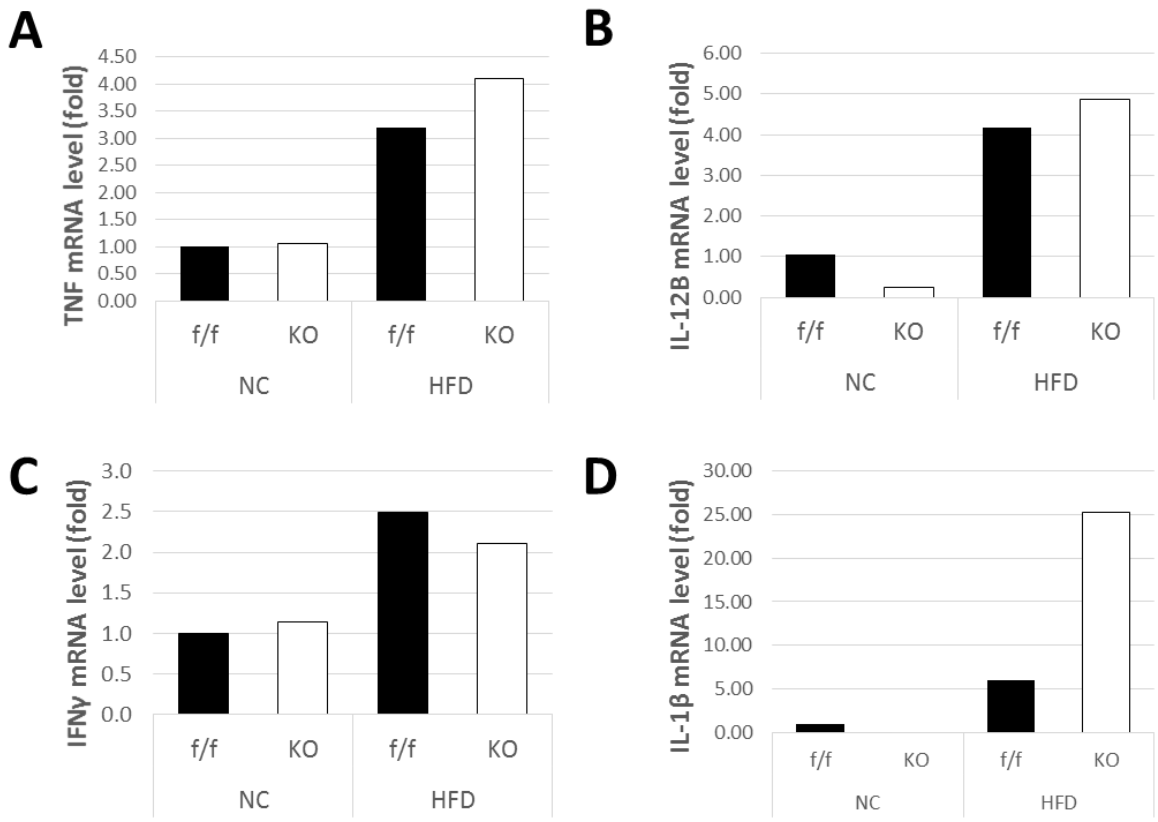

Figure 4.8: Removal of Runx2 has no effect on or increases M1 marker expression in atherosclerotic lesions.

Gene expression of M1 markers was determined by quantitative RT-PCR using pooled aortic arches. Expression of *TNF* **(A)**, *IL-12B* **(B)**, *IFNγ* **(C)**, and *IL-1β* **(D)** using quantitative RT-PCR using pooled aortic arches from pooled 18 week HFD mice (n = 3).

	Gene	$Runx2^{f/f}$ vs. $Runx2^{\Delta SM}$ (HFD)
M1	TNF	*no change*
	IL-12B	*no change*
	IFNγ	*no change*
	IL1β	+++
M2	Arg1	+++
	MRC-1	++
	Ym1	++
	IL-10	+

Table 4.1: Summary of macrophage marker changes following removal of Runx2.

Gene expression of M1 markers was determined by quantitative RT-PCR using pooled aortic arches. Changes in M1 and M2 markers were scored according to increases in $Runx2^{\Delta SM}$ expression compared to $Runx2^{f/f}$ samples. (Scale*: "+" = up to 100% increase; "++" = over 100% increase; "+++" = over 200% increase.*)

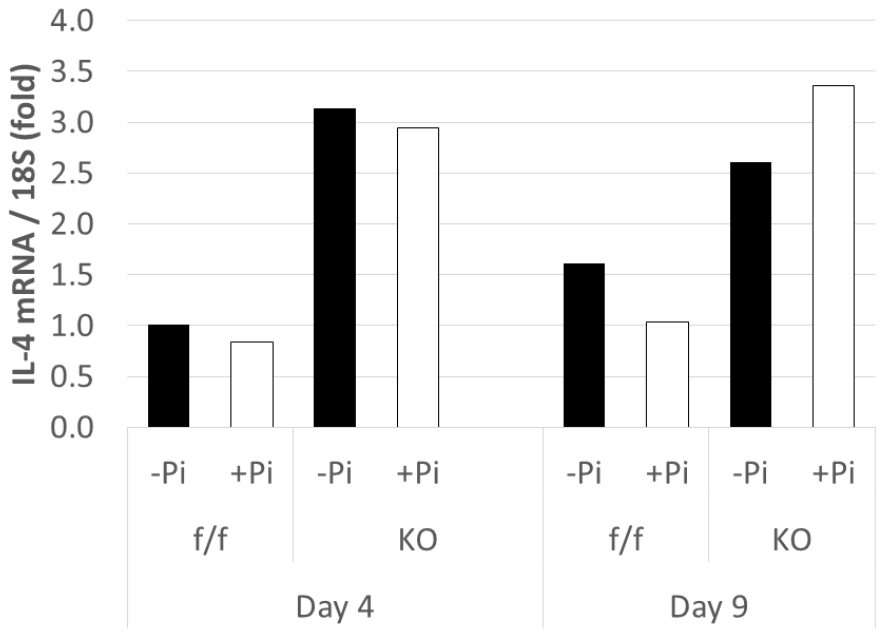

Figure 4.9: Removal of Runx2 upregulates IL-4 expression in SMCs.

Isolated Runx2$^{f/f}$ and Runx2$^{\Delta SM}$ VSMCs were cultured with or without inorganic phosphate for 4 or 9 days. RNA was extracted and *Il4* gene expression was measured by quantitative RT-PCR.

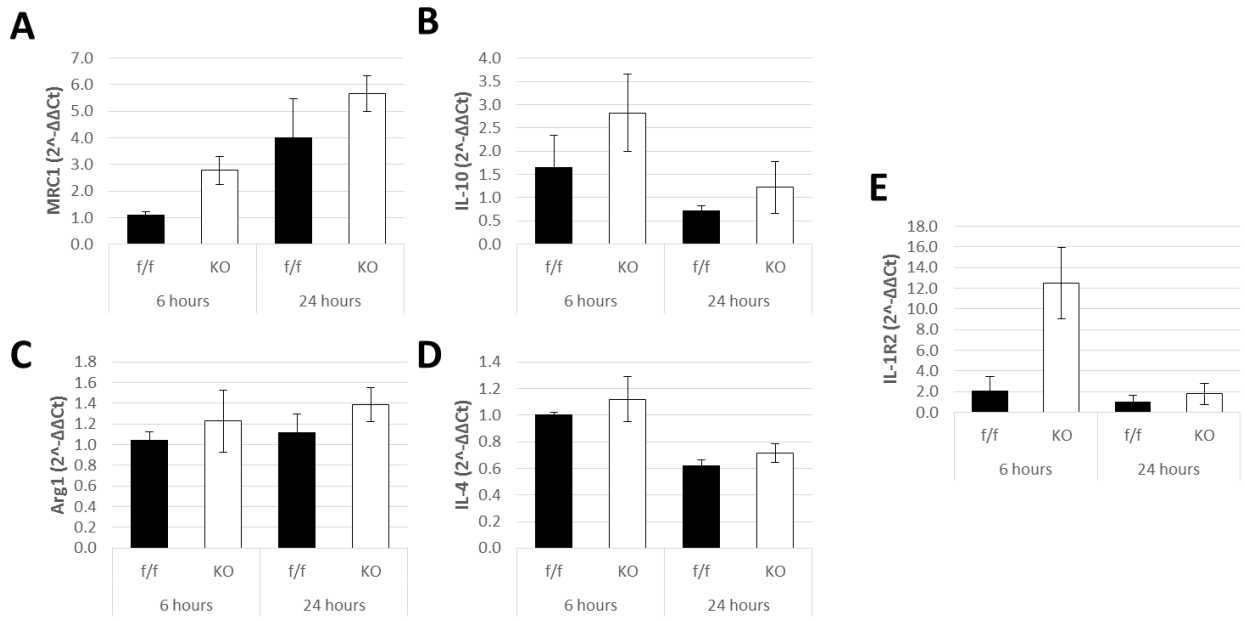

Figure 4.10: Co-culture of RAW264.7 cells and Runx2ΔSM SMCs affects M2 marker expression in RAW64.7 cells.

RAW264.7 cells were co-cultured with Runx2-f/f or KO SMCs for 6 or 24 hours. Gene expression of RAW264.7 for M2 markers was determined by quantitative RT-PCR using triplicate wells. *Arg1* **(A)**, *MRC-1* **(B)**, *Ym1* **(C)**, and *IL-10* **(D)**, and *IL-1R2* **(E)** gene expression was quantified.

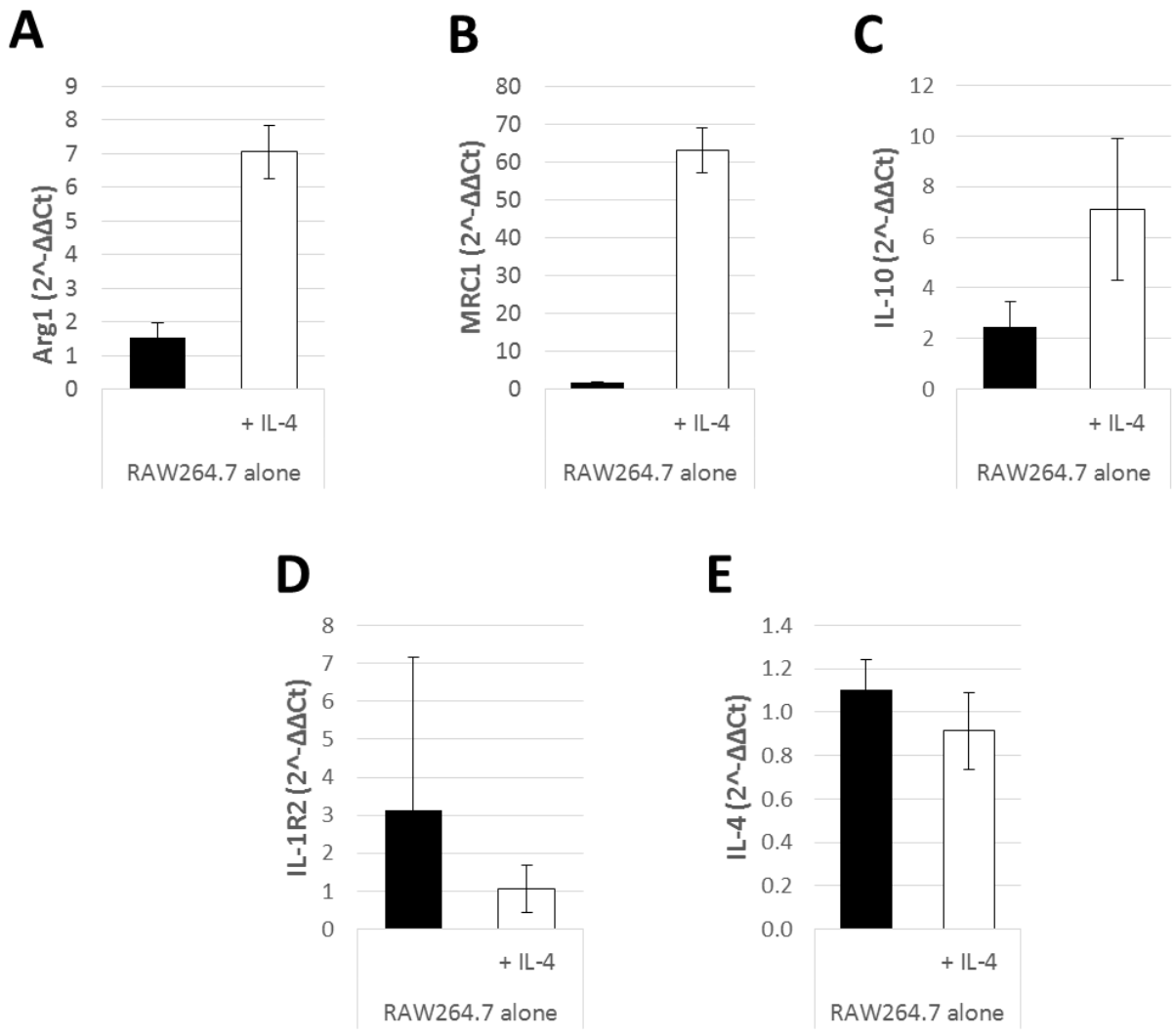

Figure 4.11: Macrophage marker expression of RAW264.7 cells induced by IL-4.

Gene expression of M1 and M2 markers was determined by quantitative RT-PCR using RAW264.7 cells induced by 50 ng/mL recombinant IL-4 in triplicate. Expression of *Arg1* **(A)**, *MRC-1* **(B)**, *IL-10* **(C)**, *IL-1R2* **(D)**, and *IL-4* **(E)** in IL-4 treated vs. untreated samples.

5 Chapter 5: Overall Conclusions

Through models for vascular medial and intimal calcification (**Chapters 2** and **3**), we have demonstrated the importance of smooth muscle-specific expression of Runx2 for osteoblastic differentiation and calcification (medial and intimal) and chondrocyte maturation (intimal). Removal of Runx2 resulted in reduced arterial calcification in both medial and intimal calcification models. Our studies showed that while SMC expression of Runx2 was not required for initial chondrogenesis in intimal calcification, it was necessary for maturation of chondrocytes to a pro-mineralizing, hypertrophic state. This research has improved upon previous work in the field by eliminating a confounding weakness to further clarify the role of smooth muscle-specific Runx2 in intimal calcification. Contrary to previous studies, we found that Runx2 did not affect monocyte/macrophage infiltration of atherosclerotic lesions despite a reduction in vascular calcification (**Chapter 4**). Additionally, we observed that removal of Runx2 did not affect atherosclerotic lesion size.

This work is also the first to propose and link Runx2 and macrophage polarization in atherosclerotic lesions and our studies are the first to show increases in M2 macrophage marker expression following SMC-specific removal of Runx2 both *in vivo* and *in vitro*. Indeed, Runx2 removal from SMCs induced a strong shift toward an M2 polarization in atherosclerotic aortas. Likewise, a co-culture model of vascular SMCs and RAW264.7 cells to study the effect of Runx2-mediated smooth muscle signaling of macrophages found significant increases in expression of two M2 markers: MRC1 and IR-1R2. To our knowledge, these results are the first to show that Runx2 and SMCs can directly alter macrophage polarization. The work in this dissertation provides an increased understanding of the role of Runx2 in multiple facets of

vascular calcification and could aid in the design of therapeutics to treat arterial calcification and atherosclerosis (**Figure 5.1**).

5.1 Figures

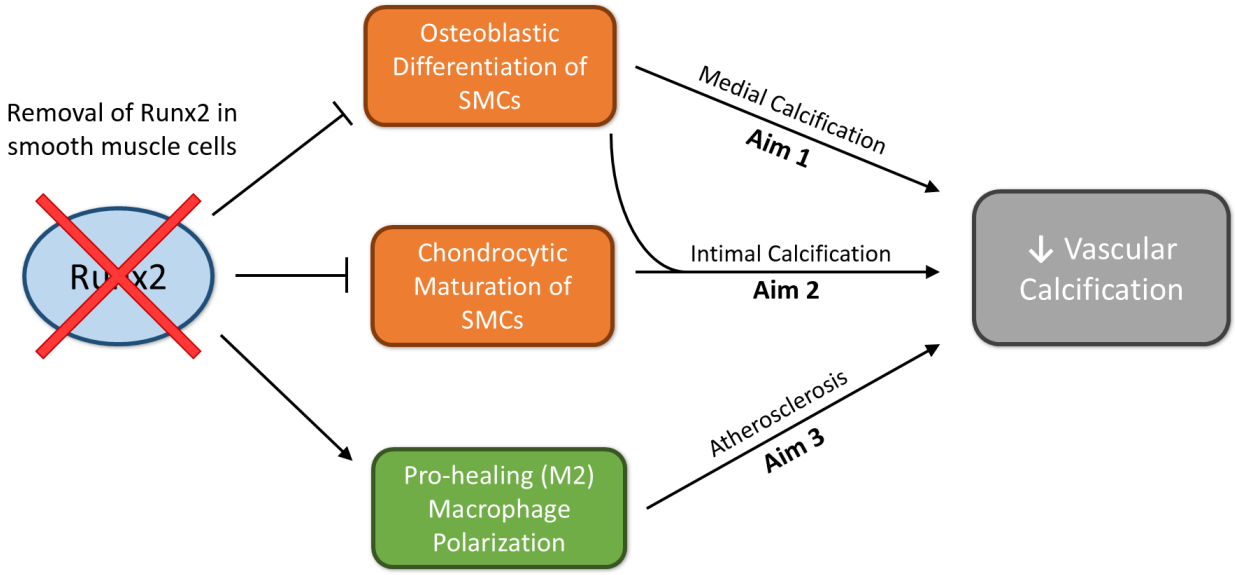

Figure 5.1: Summary of major findings

6 Chapter 6: Future Studies

The work presented in this dissertation begins to explore the role of Runx2 in AMC and AIC, as well as its role in modulating macrophage polarization in atherosclerotic lesions. Several directions for future studies are suggested below:

6.1 Determining mechanisms of Runx2-mediated macrophage polarization by SMCs

In this work, we identified effects of Runx2 on macrophage polarization both *in vivo* and *in vitro*. However, we have not identified specific targets or signaling mechanisms through which these effects occur. Studies that seek to explicate these mechanisms would improve our understanding of underlying pathologies and offer novel targets for therapeutic use.

Multiplex Luminex cytokine assays could be used to test the hypothesis that specific Th1/Th2 cytokines act as key mediators for Runx2-dependent polarization. ChIP-seq could be used to directly identify Runx2 regulatory targets, especially secreted factors and cytokines. Likewise, a proteomic approach can be used to determine whether Runx2 controls transcription by forming a complex with a co-factor (such as GATA3 or HDAC6).[111,112] Runx2 complexes can be immunoprecipitated from culture samples and analyzed via mass spectrometry to identify co-binding candidates. Proteins or molecules found using these methods can be further validated through additional studies. Lastly, Runx2-mediated SMC signaling of lesional macrophages may act primarily through cell-cell interactions via surface proteins instead of by paracrine signaling. Comparisons of membrane fractions can be analyzed via shotgun chromatography/mass spectrometry to determine differential surface expression for proteins of interest.[113]

6.2 Examining changes in macrophage polarization within atherosclerotic lesions

Key *in vivo* studies have shown that localization of M1 and M2 macrophages differ within atherosclerotic lesions.[89,95] M1 macrophages feature predominantly in the lipid core and plaque shoulders, while M2 macrophages are more commonly found in the adventitia and areas of neovascularization. Both types are present in fibrous caps. In mice, overall changes in the M1/M2 balance have been linked to plaque stability.[114] While our *in vivo* data detected broad changes in macrophage polarization within vessels with removal of Runx2, we have not considered changes within the lesion. M1 and M2 markers have been shown to localize to spatially distinct areas of early and advanced atherosclerotic lesions.[89] Indeed, some areas of the lesion are more prone to rupture (e.g. shoulder regions) and more critical for patient mortality.[115]

Are the differences in M2 marker expression in atherosclerotic lesions we observed indicative of the health of the entire lesion or of only a subset of macrophages in stable plaque areas? While M2 macrophages are primarily associated with plaque stability, it's been suggested that even a locally enhanced M1 profile could diminish lesion integrity and increase the likelihood of adverse clinical events.[89] Thus, determining whether Runx2 can modulate macrophage phenotypes within specific niches in atherosclerotic lesions could lead to development of more potent therapeutics that can more directly target regions of interest within the lesion.

7 Literature Citations

1. Thompson B, Towler D a. Arterial calcification and bone physiology: role of the bone-vascular axis. *Nat Rev Endocrinol*. 2012;8(9):529-543. doi:10.1038/nrendo.2012.36.
2. Murphy WA, Nedden D zur, Gostner P, Knapp R, Recheis W, Seidler H. The Iceman: Discovery and Imaging1. *Radiology*. 2003;226(3):614-629. doi:10.1148/radiol.2263020338.
3. Thompson RC, Allam AH, Lombardi GP, et al. Atherosclerosis across 4000 years of human history: the Horus study of four ancient populations. *Lancet*. 2013;381(9873):1211-1222. doi:10.1016/S0140-6736(13)60598-X.
4. Rosenhek R, Klaar U, Schemper M, et al. Mild and moderate aortic stenosis: Natural history and risk stratification by echocardiography. *Eur Heart J*. 2004;25:199-205. doi:10.1016/j.ehj.2003.12.002.
5. Rosenhek R, Binder T, Porenta G, et al. Predictors of outcome in severe, asymptomatic aortic stenosis. *N Engl J Med*. 2000;343:611-617. doi:10.1056/NEJM200008313430903.
6. London GM, Guérin AP, Marchais SJ, Métivier F, Pannier B, Adda H. Arterial media calcification in end-stage renal disease: Impact on all-cause and cardiovascular mortality. *Nephrol Dial Transplant*. 2003;18:1731-1740. doi:10.1093/ndt/gfg414.
7. Lehto S, Niskanen L, Suhonen M, Rönnemaa T, Laakso M. Medial artery calcification. A neglected harbinger of cardiovascular complications in non-insulin-dependent diabetes mellitus. *Arterioscler Thromb Vasc Biol*. 1996;16:978-983. doi:10.1161/01.ATV.16.8.978.
8. Demer LL, Tintut Y. Vascular calcification: pathobiology of a multifaceted disease. *Circulation*. 2008;117(22):2938-2948. doi:10.1161/CIRCULATIONAHA.107.743161.

9. Wu M, Rementer C, Giachelli CM. Vascular calcification: An update on mechanisms and challenges in treatment. *Calcif Tissue Int*. 2013;93:365-373. doi:10.1007/s00223-013-9712-z.

10. Mohler ER, Gannon F, Reynolds C, Zimmerman R, Keane MG, Kaplan FS. Bone formation and inflammation in cardiac valves. *Circulation*. 2001;103:1522-1528. doi:10.1161/01.CIR.103.11.1522.

11. Tyson KL, Reynolds JL, McNair R, Zhang Q, Weissberg PL, Shanahan CM. Osteo/chondrocytic transcription factors and their target genes exhibit distinct patterns of expression in human arterial calcification. *Arterioscler Thromb Vasc Biol*. 2003;23(3):489-494. doi:10.1161/01.ATV.0000059406.92165.31.

12. Schulick AH, Taylor AJ, Zuo W, et al. Overexpression of transforming growth factor beta1 in arterial endothelium causes hyperplasia, apoptosis, and cartilaginous metaplasia. *Proc Natl Acad Sci U S A*. 1998;95:6983-6988. doi:10.1073/pnas.95.12.6983.

13. Bobryshev Y V. Transdifferentiation of smooth muscle cells into chondrocytes in atherosclerotic arteries in situ: Implications for diffuse intimal calcification. *J Pathol*. 2005;205(5):641-650. doi:10.1002/path.1743.

14. Shanahan CM, Cary NR, Salisbury JR, Proudfoot D, Weissberg PL, Edmonds ME. Medial localization of mineralization-regulating proteins in association with Mönckeberg's sclerosis: evidence for smooth muscle cell-mediated vascular calcification. *Circulation*. 1999;100(21):2168-2176. doi:10.1161/01.CIR.100.21.2168.

15. Neven E, Dauwe S, De Broe ME, D'Haese PC, Persy V. Endochondral bone formation is involved in media calcification in rats and in men. *Kidney Int*. 2007;72:574-581. doi:10.1038/sj.ki.5002353.

16. Aikawa E, Nahrendorf M, Figueiredo J-L, et al. Osteogenesis associates with inflammation in early-stage atherosclerosis evaluated by molecular imaging in vivo. *Circulation*. 2007;116(24):2841-2850. doi:10.1161/CIRCULATIONAHA.107.732867.

17. Guzman RJ, Brinkley DM, Schumacher PM, Donahue RMJ, Beavers H, Qin X. Tibial Artery Calcification as a Marker of Amputation Risk in Patients With Peripheral Arterial Disease. *J Am Coll Cardiol*. 2008;51:1967-1974. doi:10.1016/j.jacc.2007.12.058.

18. Olson JC, Edmundowicz D, Becker DJ, Kuller LH, Orchard TJ. Coronary calcium in adults with type 1 diabetes: A stronger correlate of clinical coronary artery disease in men than in women. *Diabetes*. 2000;49:1571-1578. doi:10.2337/diabetes.49.9.1571.

19. Pannier B, Guérin AP, Marchais SJ, Safar ME, London GM. Stiffness of capacitive and conduit arteries: Prognostic significance for end-stage renal disease patients. *Hypertension*. 2005;45(4):592-596. doi:10.1161/01.HYP.0000159190.71253.c3.

20. Fitzgerald PJ, Ports TA, Yock PG. Contribution of localized calcium deposits to dissection after angioplasty. An observational study using intravascular ultrasound. *Circulation*. 1992;86:64-70. doi:10.1161/01.CIR.86.1.64.

21. Ehara S, Kobayashi Y, Yoshiyama M, et al. Spotty calcification typifies the culprit plaque in patients with acute myocardial infarction: An intravascular ultrasound study. *Circulation*. 2004;110:3424-3429. doi:10.1161/01.CIR.0000148131.41425.E9.

22. Loecker TH, Schwartz RS, Cotta CW, Hickman JR. Fluoroscopic coronary artery calcification and associated coronary disease in asymptomatic young men. *J Am Coll Cardiol*. 1992;19:1167-1172. doi:10.1016/0735-1097(92)90319-I.

23. Vihert AM. Atherosclerosis of the aorta and coronary arteries in coronary heart disease. *Bull World Health Organ*. 1976;53:585-596.

24. Vliegenthart R, Hollander M, Breteler MMB, et al. Stroke is associated with coronary calcification as detected by electron-beam CT: The Rotterdam Coronary Calcification Study. *Stroke*. 2002;33:462-465. doi:10.1161/hs0202.103071.

25. Peled M, Fisher E a. Dynamic Aspects of Macrophage Polarization during Atherosclerosis Progression and Regression. *Front Immunol*. 2014;5(November):1-9. doi:10.3389/fimmu.2014.00579.

26. Mozaffarian D, Benjamin EJ, Go a. S, et al. *Heart Disease and Stroke Statistics--2015 Update: A Report From the American Heart Association*.; 2014. doi:10.1161/CIR.0000000000000152.

27. Mundlos S, Otto F, Mundlos C, et al. Mutations involving the transcription factor CBFA1 cause cleidocranial dysplasia. *Cell*. 1997;89:773-779. doi:10.1016/S0092-8674(00)80260-3.

28. Otto F, Thornell AP, Crompton T, et al. Cbfa1, a candidate gene for cleidocranial dysplasia syndrome, is essential for osteoblast differentiation and bone development. *Cell*. 1997;89:765-771. doi:10.1016/S0092-8674(00)80259-7.

29. Komori T, Yagi H, Nomura S, et al. Targeted disruption of Cbfa1 results in a complete lack of bone formation owing to maturational arrest of osteoblasts. *Cell*. 1997;89(5):755-764. doi:10.1016/S0092-8674(00)80258-5.

30. Chen H, Ghori-Javed FY, Rashid H, et al. Runx2 Regulates Endochondral Ossification through Control of Chondrocyte Proliferation and Differentiation. *J Bone Miner Res*. 2014;29(12):1-33. doi:10.1002/jbmr.2287.

31. Olsen BR, Reginato AM, Wang W. Bone development. *Annu Rev Cell Dev Biol*. 2000;16:191-220. doi:10.1146/annurev.cellbio.16.1.191.

32. Karsenty G, Wagner EF. Reaching a genetic and molecular understanding of skeletal development. *Dev Cell*. 2002;2:389-406. doi:10.1016/S1534-5807(02)00157-0.

33. Ducy P, Zhang R, Geoffroy V, Ridall AL, Karsenty G. Osf2/Cbfa1: a transcriptional activator of osteoblast differentiation. *Cell*. 1997;89:747-754. doi:10.1016/S0092-8674(00)80257-3.

34. Nishio Y, Dong Y, Paris M, O'Keefe RJ, Schwarz EM, Drissi H. Runx2-mediated regulation of the zinc finger Osterix/Sp7 gene. *Gene*. 2006;372:62-70. doi:10.1016/j.gene.2005.12.022.

35. Harada H, Tagashira S, Fujiwara M, et al. Cbfa1 isoforms exert functional differences in osteoblast differentiation. *J Biol Chem*. 1999;274:6972-6978. doi:10.1074/jbc.274.11.6972.

36. Zheng Q, Zhou G, Morello R, Chen Y, Garcia-Rojas X, Lee B. Type X collagen gene regulation by Runx2 contributes directly to its hypertrophic chondrocyte-specific expression in vivo. *J Cell Biol*. 2003;162(5):833-842. doi:10.1083/jcb.200211089.

37. Vimalraj S, Arumugam B, Miranda PJ, Selvamurugan N. Runx2: Structure, Function, and Phosphorylation in Osteoblast Differentiation. *Int J Biol Macromol*. 2015;78:202-208. doi:10.1016/j.ijbiomac.2015.04.008.

38. Bruderer M, Richards RG, Alini M, Stoddart MJ. Role and regulation of RUNX2 in osteogenesis. *Eur Cell Mater*. 2014;28:269-286. http://www.ncbi.nlm.nih.gov/pubmed/25340806.

39. Ziros PG, Basdra EK, Papavassiliou AG. Runx2: of bone and stretch. *Int J Biochem Cell Biol*. 2008;40(9):1659-1663. doi:10.1016/j.biocel.2007.05.024.

40. Ge C, Xiao G, Jiang D, et al. Identification and functional characterization of ERK/MAPK

phosphorylation sites in the Runx2 transcription factor. *J Biol Chem*. 2009;284(47):32533-32543. doi:10.1074/jbc.M109.040980.

41. Li Y, Ge C, Long JP, et al. Biomechanical stimulation of osteoblast gene expression requires phosphorylation of the RUNX2 transcription factor. *J Bone Miner Res*. 2012;27(6):1263-1274. doi:10.1002/jbmr.1574.

42. Shroff RC, McNair R, Figg N, et al. Dialysis accelerates medial vascular calcification in part by triggering smooth muscle cell apoptosis. *Circulation*. 2008;118:1748-1757. doi:10.1161/CIRCULATIONAHA.108.783738.

43. Naik V, Leaf EM, Hu JH, et al. Sources of cells that contribute to atherosclerotic intimal calcification: an in vivo genetic fate mapping study. *Cardiovasc Res*. 2012;94(3):545-554. doi:10.1093/cvr/cvs126.

44. Speer MY, Yang H-Y, Brabb T, et al. Smooth muscle cells give rise to osteochondrogenic precursors and chondrocytes in calcifying arteries. *Circ Res*. 2009;104(6):733-741. doi:10.1161/CIRCRESAHA.108.183053.

45. Tanaka T, Sato H, Doi H, et al. Runx2 represses myocardin-mediated differentiation and facilitates osteogenic conversion of vascular smooth muscle cells. *Mol Cell Biol*. 2008;28(3):1147-1160. doi:10.1128/MCB.01771-07.

46. Nakahara T, Sato H, Shimizu T, et al. Fibroblast growth factor-2 induces osteogenic differentiation through a Runx2 activation in vascular smooth muscle cells. *Biochem Biophys Res Commun*. 2010;394(2):243-248. doi:10.1016/j.bbrc.2009.11.038.

47. Speer MY, Li X, Hiremath PG, Giachelli CM. Runx2/Cbfa1, but not loss of myocardin, is required for smooth muscle cell lineage reprogramming toward osteochondrogenesis. *J Cell Biochem*. 2010;110(4):935-947. doi:10.1002/jcb.22607.

48. Han MS, Che X, Cho GH, et al. Functional cooperation between vitamin D receptor and Runx2 in vitamin D-induced vascular calcification. *PLoS One*. 2013;8(12):1-14. doi:10.1371/journal.pone.0083584.

49. Sun Y, Byon CH, Yuan K, et al. Smooth muscle cell-specific Runx2 deficiency inhibits vascular calcification. *Circ Res*. 2012;111(5):543-552. doi:10.1161/CIRCRESAHA.112.267237.

50. Adhami MD, Rashid H, Chen H, Clarke JC, Yang Y, Javed A. Loss of Runx2 in Committed Osteoblasts Impairs Postnatal Skeletogenesis. *J Bone Miner Res*. 2015;30(1):71-82. doi:10.1002/jbmr.2321.

51. Thirunavukkarasu K, Mahajan M, McLarren KW, Stifani S, Karsenty G. Two domains unique to osteoblast-specific transcription factor Osf2/Cbfa1 contribute to its transactivation function and its inability to heterodimerize with Cbfbeta. *Mol Cell Biol*. 1998;18(7):4197-4208. http://www.ncbi.nlm.nih.gov/pubmed/9632804.

52. Nguyen N, Naik V, Speer MY. Diabetes mellitus accelerates cartilaginous metaplasia and calcification in atherosclerotic vessels of LDLr mutant mice. *Cardiovasc Pathol*. 2013;22(2):167-175. doi:10.1016/j.carpath.2012.06.007.

53. Yao Y, Jumabay M, Ly A, Radparvar M, Cubberly MR, Boström KI. A role for the endothelium in vascular calcification. *Circ Res*. 2013;113(5):495-504. doi:10.1161/CIRCRESAHA.113.301792.

54. New SEP, Goettsch C, Aikawa M, et al. Macrophage-Derived Matrix Vesicles: An Alternative Novel Mechanism for Microcalcification in Atherosclerotic Plaques. *Circ Res*. 2013;113(1):72-77. doi:10.1161/CIRCRESAHA.113.301036.

55. Liao J, Chen X, Li Y, et al. Transfer of bone-marrow-derived mesenchymal stem cells

influences vascular remodeling and calcification after balloon injury in hyperlipidemic rats. *J Biomed Biotechnol*. 2012;2012. doi:10.1155/2012/165296.

56. Steitz SA, Speer MY, Curinga G, et al. Smooth Muscle Cell Phenotypic Transition Associated With Calcification: Upregulation of Cbfa1 and Downregulation of Smooth Muscle Lineage Markers. *Circ Res*. 2001;89(12):1147-1154. doi:10.1161/hh2401.101070.

57. Frutkin AD, Shi H, Otsuka G, Levéen P, Karlsson S, Dichek DA. A critical developmental role for tgfbr2 in myogenic cell lineages is revealed in mice expressing SM22-Cre, not SMMHC-Cre. *J Mol Cell Cardiol*. 2006;41:724-731. doi:10.1016/j.yjmcc.2006.06.067.

58. Holtwick R, Gotthardt M, Skryabin B, et al. Smooth muscle-selective deletion of guanylyl cyclase-A prevents the acute but not chronic effects of ANP on blood pressure. *Proc Natl Acad Sci U S A*. 2002;99:7142-7147. doi:10.1073/pnas.102650499.

59. Kang YH, Jin JS, Yi DW, Son SM. Bone morphogenetic protein-7 inhibits vascular calcification induced by high vitamin D in mice. *Tohoku J Exp Med*. 2010;221:299-307. doi:10.1620/tjem.221.299.

60. Pai A, Leaf EM, El-Abbadi M, Giachelli CM. Elastin Degradation and Vascular Smooth Muscle Cell Phenotype Change Precede Cell Loss and Arterial Medial Calcification in a Uremic Mouse Model of Chronic Kidney Disease. *Am J Pathol*. 2011;178(2):764-773. doi:10.1016/j.ajpath.2010.10.006.

61. Li L, Miano JM, Mercer B, Olson EN. Expression of the SM22alpha promoter in transgenic mice provides evidence for distinct transcriptional regulatory programs in vascular and visceral smooth muscle cells. *J Cell Biol*. 1996;132(5):849-859. http://www.pubmedcentral.nih.gov/articlerender.fcgi?artid=2120743&tool=pmcentrez&rendertype=abstract. Accessed September 11, 2014.

62. Quarles LD. Role of FGF23 in vitamin D and phosphate metabolism: implications in chronic kidney disease. *Exp Cell Res*. 2012;318(9):1040-1048. doi:10.1016/j.yexcr.2012.02.027.

63. Zebger-Gong H, Müller D, Diercke M, et al. 1,25-Dihydroxyvitamin D3-induced aortic calcifications in experimental uremia: up-regulation of osteoblast markers, calcium-transporting proteins and osterix. *J Hypertens*. 2011;29(2):339-348. doi:10.1097/HJH.0b013e328340aa30.

64. Moe SM, Duan D, Doehle BP, O'Neill KD, Chen NX. Uremia induces the osteoblast differentiation factor Cbfa1 in human blood vessels. *Kidney Int*. 2003;63(3):1003-1011. doi:10.1046/j.1523-1755.2003.00820.x.

65. Mathew S, Lund RJ, Chaudhary LR, Geurs T, Hruska KA. Vitamin D Receptor Activators Can Protect against Vascular Calcification. *J Am Soc Nephrol*. 2008;19(8):1509-1519. doi:10.1681/ASN.2007080902.

66. Giachelli CM. The emerging role of phosphate in vascular calcification. *Kidney Int*. 2009;75(9):890-897. doi:10.1038/ki.2008.644.

67. Ducy P, Starbuck M, Priemel M, et al. A Cbfa1-dependent genetic pathway controls bone formation beyond embryonic development. *Genes Dev*. 1999;13:1025-1036. doi:10.1101/gad.13.8.1025.

68. Rosenbauer F, Tenen DG. Transcription factors in myeloid development: balancing differentiation with transformation. *Nat Rev Immunol*. 2007;7:105-117. doi:10.1038/nri2024.

69. Estecha A, Aguilera-Montilla N, Sánchez-Mateos P, Puig-Kröger A. Runx3 regulates intercellular adhesion molecule 3 (icam-3) expression during macrophage differentiation

and monocyte extravasation. *PLoS One*. 2012;7(3). doi:10.1371/journal.pone.0033313.

70. Woolf E, Xiao C, Fainaru O, et al. Runx3 and Runx1 are required for CD8 T cell development during thymopoiesis. *Proc Natl Acad Sci U S A*. 2003;100:7731-7736. doi:10.1073/pnas.1232420100.

71. Fujita T, Azuma Y, Fukuyama R, et al. Runx2 induces osteoblast and chondrocyte differentiation and enhances their migration by coupling with PI3K-Akt signaling. *J Cell Biol*. 2004;166:85-95. doi:10.1083/jcb.200401138.

72. Enomoto H, Furuichi T, Zanma A, et al. Runx2 deficiency in chondrocytes causes adipogenic changes in vitro. *J Cell Sci*. 2004;117(Pt 3):417-425. doi:10.1242/jcs.00866.

73. Hinoi E, Bialek P, Chen YT, et al. Runx2 inhibits chondrocyte proliferation and hypertrophy through its expression in the perichondrium. *Genes Dev*. 2006;20:2937-2942. doi:10.1101/gad.1482906.

74. Dong YF, Soung DY, Schwarz EM, O'Keefe RJ, Drissi H. Wnt induction of chondrocyte hypertrophy through the Runx2 transcription factor. *J Cell Physiol*. 2006;208:77-86. doi:10.1002/jcp.20656.

75. Yoshida T, Gan Q, Franke AS, et al. Smooth and cardiac muscle-selective knock-out of Kruppel-like factor 4 causes postnatal death and growth retardation. *J Biol Chem*. 2010;285(27):21175-21184. doi:10.1074/jbc.M110.112482.

76. Takarada T, Hinoi E, Nakazato R, et al. An analysis of skeletal development in osteoblast-specific and chondrocyte-specific runt-related transcription factor-2 (Runx2) knockout mice. *J Bone Miner Res*. 2013;28(10):2064-2069. doi:10.1002/jbmr.1945.

77. Akiyama H, Chaboissier M-C, Martin JF, Schedl A, de Crombrugghe B. The transcription factor Sox9 has essential roles in successive steps of the chondrocyte differentiation

pathway and is required for expression of Sox5 and Sox6. *Genes Dev*. 2002;16(21):2813-2828. doi:10.1101/gad.1017802.

78. Dy P, Wang W, Bhattaram P, et al. Sox9 Directs Hypertrophic Maturation and Blocks Osteoblast Differentiation of Growth Plate Chondrocytes. *Dev Cell*. 2012;22(3):597-609. doi:10.1016/j.devcel.2011.12.024.

79. Lin M-E, Chen TM, Leaf EM, et al. Runx2 Expression in Smooth Muscle Cells Is Required for Arterial Medial Calcification in Mice. *Am J Pathol*. 2014;185(7):1958-1969. doi:10.1016/j.ajpath.2015.03.020.

80. Pai AS, Giachelli CM. Matrix remodeling in vascular calcification associated with chronic kidney disease. *J Am Soc Nephrol*. 2010;21(10):1637-1640. doi:10.1681/ASN.2010040349.

81. Byon CH, Javed A, Dai Q, et al. Oxidative stress induces vascular calcification through modulation of the osteogenic transcription factor Runx2 by AKT signaling. *J Biol Chem*. 2008;283(22):15319-15327. doi:10.1074/jbc.M800021200.

82. Yamashita S, Andoh M, Ueno-Kudoh H, Sato T, Miyaki S, Asahara H. Sox9 directly promotes Bapx1 gene expression to repress Runx2 in chondrocytes. *Exp Cell Res*. 2009;315(13):2231-2240. doi:10.1016/j.yexcr.2009.03.008.

83. Hartmann C. Transcriptional networks controlling skeletal development. *Curr Opin Genet Dev*. 2009;19(5):437-443. doi:10.1016/j.gde.2009.09.001.

84. Liu T, Gao Y, Sakamoto K, et al. BMP-2 promotes differentiation of osteoblasts and chondroblasts in Runx2-deficient cell lines. *J Cell Physiol*. 2007;211(3):728-735. doi:10.1002/jcp.20988.

85. van der Wal AC, Becker AE. Atherosclerotic plaque rupture--pathologic basis of plaque

stability and instability. *Cardiovasc Res*. 1999;41:334-344. doi:S0008-6363(98)00276-4 [pii].

86. Moore KJ, Sheedy FJ, Fisher E a. Macrophages in atherosclerosis: a dynamic balance. *Nat Rev Immunol*. 2013;13(10):709-721. doi:10.1038/nri3520.

87. Moore KJ, Tabas I. Macrophages in the pathogenesis of atherosclerosis. *Cell*. 2011;145(3):341-355. doi:10.1016/j.cell.2011.04.005.

88. Colin S, Chinetti-Gbaguidi G, Staels B. Macrophage phenotypes in atherosclerosis. *Immunol Rev*. 2014;262(1):153-166. doi:10.1111/imr.12218.

89. Stöger JL, Gijbels MJJ, van der Velden S, et al. Distribution of macrophage polarization markers in human atherosclerosis. *Atherosclerosis*. 2012;225:461-468. doi:10.1016/j.atherosclerosis.2012.09.013.

90. Deuell KA, Callegari A, Giachelli CM, Rosenfeld ME, Scatena M. RANKL enhances macrophage paracrine pro-calcific activity in high phosphate-treated smooth muscle cells: dependence on IL-6 and TNF-α. *J Vasc Res*. 2012;49(6):510-521. doi:10.1159/000341216.

91. Hénaut L, Sanchez-Nino MD, Aldamiz-Echevarría Castillo G, Sanz AB, Ortiz A. Targeting local vascular and systemic consequences of inflammation on vascular and cardiac valve calcification. *Expert Opin Ther Targets*. 2016;20(1):89-105. doi:10.1517/14728222.2015.1081685.

92. Chinetti-Gbaguidi G, Baron M, Bouhlel MA, et al. Human atherosclerotic plaque alternative macrophages display low cholesterol handling but high phagocytosis because of distinct activities of the PPARγ and LXRα pathways. *Circ Res*. 2011;108:985-995. doi:10.1161/CIRCRESAHA.110.233775.

93. Harmon EY, Fronhofer V, Keller RS, et al. Anti-Inflammatory Immune Skewing Is Atheroprotective: Apoe-/-Fc RIIb-/- Mice Develop Fibrous Carotid Plaques. *J Am Heart Assoc*. 2014;3(6):e001232-e001232. doi:10.1161/JAHA.114.001232.

94. Kadl A, Meher AK, Sharma PR, et al. Identification of a Novel Macrophage Phenotype That Develops in Response to Atherogenic Phospholipids via Nrf2. *Circ Res*. 2010;107(6):737-746. doi:10.1161/CIRCRESAHA.109.215715.

95. Chinetti-Gbaguidi G, Colin S, Staels B. Macrophage subsets in atherosclerosis. *Nat Rev Cardiol*. 2014;12(1):10-17. doi:10.1038/nrcardio.2014.173.

96. Ling G, Kalanuria, Nyquist. The prevention and regression of atherosclerotic plaques: emerging treatments. *Vasc Health Risk Manag*. 2012;8(1):549. doi:10.2147/VHRM.S27764.

97. Bessueille L, Magne D. Inflammation: a culprit for vascular calcification in atherosclerosis and diabetes. *Cell Mol Life Sci*. 2015;72(13):2475-2489. doi:10.1007/s00018-015-1876-4.

98. Averill MM, Barnhart S, Becker L, et al. S100A9 Differentially Modifies Phenotypic States of Neutrophils, Macrophages, and Dendritic Cells: Implications for Atherosclerosis and Adipose Tissue Inflammation. *Circulation*. 2011;123(11):1216-1226. doi:10.1161/CIRCULATIONAHA.110.985523.

99. Park S-J, Lee K-P, Kang S, et al. Sphingosine 1-phosphate induced anti-atherogenic and atheroprotective M2 macrophage polarization through IL-4. *Cell Signal*. 2014;26(10):2249-2258. doi:10.1016/j.cellsig.2014.07.009.

100. Boyce BF, Xing L. Functions of RANKL/RANK/OPG in bone modeling and remodeling. *Arch Biochem Biophys*. 2008;473(2):139-146. doi:10.1016/j.abb.2008.03.018.

101. Breuil V, Schmid-Antomarchi H, Schmid-Alliana A, Rezzonico R, Euller-Ziegler L, Rossi B. The receptor activator of nuclear factor (NF)-kappaB ligand (RANKL) is a new chemotactic factor for human monocytes. *FASEB J*. 2003;17(12):1751-1753. doi:10.1096/fj.02-1188fje.

102. Mantovani A, Sica A, Sozzani S, Allavena P, Vecchi A, Locati M. The chemokine system in diverse forms of macrophage activation and polarization. *Trends Immunol*. 2004;25(12):677-686. doi:10.1016/j.it.2004.09.015.

103. Alexander MR, Moehle CW, Johnson JL, et al. Genetic inactivation of IL-1 signaling enhances atherosclerotic plaque instability and reduces outward vessel remodeling in advanced atherosclerosis in mice. *J Clin Invest*. 2012;122(1):70-79. doi:10.1172/JCI43713.

104. Conlon PJ, Tyler S, Grabstein KH, Morrissey P. Interleukin-4 (B-cell stimulatory factor-1) augments the in vivo generation of cytotoxic cells in immunosuppressed animals. *Biotechnol Ther*. 1989;1(1):31-41.

105. Gea-Sorlí S, Closa D. In vitro, but not in vivo, reversibility of peritoneal macrophages activation during experimental acute pancreatitis. *BMC Immunol*. 2009;10:42. doi:10.1186/1471-2172-10-42.

106. Brown MA. IL-4 Production by T Cells: You Need a Little to Get a Lot. *J Immunol*. 2008;181(5):2941-2942. doi:10.4049/jimmunol.181.5.2941.

107. Peters V a., Joesting JJ, Freund GG. IL-1 receptor 2 (IL-1R2) and its role in immune regulation. *Brain Behav Immun*. 2013;32:1-8. doi:10.1016/j.bbi.2012.11.006.

108. Pou J, Martínez-González J, Rebollo A, et al. Type II interleukin-1 receptor expression is reduced in monocytes/macrophages and atherosclerotic lesions. *Biochim Biophys Acta* -

Mol Cell Biol Lipids. 2011;1811(9):556-563. doi:10.1016/j.bbalip.2011.05.014.

109. Tedgui A, Ait-Oufella H, Mallat Z. Cytokines and Atherosclerosis. In: *Atherosclerosis*. Wiley-VCH Verlag GmbH & Co. KGaA; 2010:63-84. doi:10.1002/9783527629589.ch4.

110. Mantovani A, Garlanda C, Locati M. Macrophage diversity and polarization in atherosclerosis: A question of balance. *Arterioscler Thromb Vasc Biol*. 2009;29(10):1419-1423. doi:10.1161/ATVBAHA.108.180497.

111. Wei G, Abraham BJ, Yagi R, et al. Genome-wide Analyses of Transcription Factor GATA3-Mediated Gene Regulation in Distinct T Cell Types. *Immunity*. 2011;35(2):299-311. doi:10.1016/j.immuni.2011.08.007.

112. Westendorf JJ, Zaidi SK, Cascino JE, et al. Runx2 (Cbfa1, AML-3) Interacts with Histone Deacetylase 6 and Represses the p21CIP1/WAF1 Promoter. *Mol Cell Biol*. 2002;22(22):7982-7992. doi:10.1128/MCB.22.22.7982-7992.2002.

113. Wu CC, Yates JR. The application of mass spectrometry to membrane proteomics. *Nat Biotechnol*. 2003;21(3):262-267. doi:10.1038/nbt0303-262.

114. Feig JE, Parathath S, Rong JX, et al. Reversal of Hyperlipidemia With a Genetic Switch Favorably Affects the Content and Inflammatory State of Macrophages in Atherosclerotic Plaques. *Circulation*. 2011;123(9):989-998. doi:10.1161/CIRCULATIONAHA.110.984146.

115. Barlis P, Serruys PW, DeVries A, Regar E. Optical coherence tomography assessment of vulnerable plaque rupture: predilection for the plaque “shoulder.” *Eur Heart J*. 2008;29(16):2023-2023. doi:10.1093/eurheartj/ehn085.

Vita

Theodore Ming-Chien Chen was born in Atlanta, GA in 1988. He graduated from The Westminster Schools in 2006. Afterwards, he went on to attend the Georgia Institute of Technology, where he graduated with highest honors in 2009 with a Bachelors of Science in Biomedical Engineering and a minor in Chinese.

In 2010, he moved to Seattle, Washington to pursue his Ph.D. in Bioengineering at the University of Washington. In January 2011, he joined the lab of Dr. Cecilia Giachelli and Dr. Yanfeng (Mei) Speer. In May 2016, he completed his Ph.D. dissertation titled “Runx2 and vascular calcification.”